ARCHIVES OF ACOUSTICS
1, 4, 257-268 (1976)

DETERMINATION OF THE LOCATION OF SONIC BOOM

RUFIN MAKAREWICZ

Department of Acoustics of A. Mickiewicz University (Poznań)

In the paper the results of theoretical considerations which permit to determine the location of sonic boom of shock wave produced during supersonic flight are given. It has been assumed that the earth's atmosphere is a stratified medium in which the velocity of sound propagation as well as wind velocity are magnitudes which depend only on the height. For general case (at arbitrary manoeuvring of aircraft) a procedure algorithm has been defined which permits to predict the boundary of audibility area. It has also been proved that for certain types of manoeuvring (including also rectilinear flight), defined by condition (9), this algorithm enables the determination of coordinates of audibility area (grazing points) (x_A, y_A) as well as (x_B, y_B) in the analytical form (10). In the case of still atmosphere the obtained results are simplified to a well-known relation (13) determining the width of audibility belt of a shock wave.

1. Introduction

A plane flying at a supersonic velocity speed is a source of a sound shock wave. This wave has bad effects upon the people, biological life, buildings as well as upon the equipment on the earth's surface. Having this in mind, experiments have for long been conducted aimed at establishing the method of the determination of the intensivity and audibility area of this wave. Both problems can be looked upon jointly and then the audibility area of the shock wave constitutes a set of singular points encountered in equations describing the shock strength. Relevant calculations are very complex.

In many practical problems (regional planning) the problem of the audibility area is very important, e.g. in the case where, one has to do with areas (hospitals, sanatoria etc.) to which even the slightest shock wave should not reach.

Many authors have been engaged in the problem of location of sonic boom at supersonic flights, among others BARLETT and FRIEDMANN [1], HAYES and RUNYAN [6], LANSING [9], WANNER [12] as well as WARREN [13]. In

said papers, as also in this one, theoretical deliberations are based on the perception that the boundary of the audibility area is a set of tangential points to earth's surface (Fig. 2). For a general case (arbitrary manoeuvring aircraft in presence of wind) the above-mentioned papers contain the algorithm which can be evaluated by use of quick operating computers. It has been shown in this paper that the satisfaction of a certain condition that limits somewhat the freedom of the manoeuvre (9) leads to simple relations (10) which determine the coordinates of tangential points (x_A, y_A) as well as (x_B, y_B) (Fig. 2).

2. Equations of acoustic rays

In direct proximity of a plane the shock wave forms the Mach's cone. It can be thought that each point of the cone's surface is the end of the ray emitted from the cone's apex at an earlier moment (Fig. 1). The set of all rays

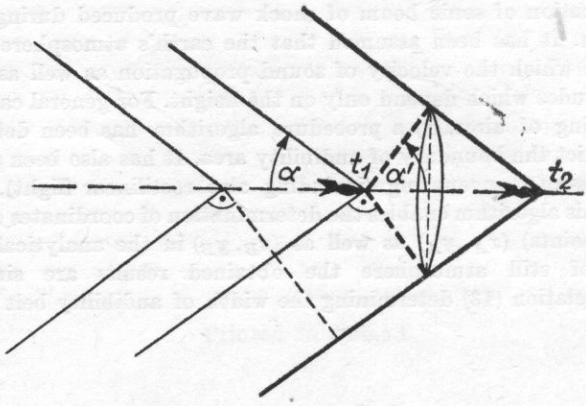

Fig. 1. Mach cone and coupled cone with obtuse angle α'

emitted at the moment t_1, the ends of which are on the surface of the cone at the moment t_2 (where $t_2 > t_1$) forms a coupled cone with obtuse angle

$$\alpha' = \frac{1}{2}\pi - \arcsin\frac{a(h)}{V},$$

whose generating lines perpendicular to Mach's cone. These generating lines are radii. Since the atmosphere is heterogeneous and anisotropic (presence of wind), these lines are curves. Some of them intersect the earth's surface and can then be heard at these points as shock waves.

The points of intersection (dashed lines on the plane x, y — Fig.2) are the axis of the influence zone of the shock wave at a certain moment. The purpose of our deliberations is to find the boundary of the audibility area not at one given moment, but over a length of time during which the influence zone moves forming a belt as shown in Fig. 2.

For the «coupled cone» there exist two radii tangent to the earth's surface φ_A and φ_B which limit the set of radii intersecting the earth's surface. In this manner the tangential points changing continuously in time form the boundary of the audibility area supersonic flight.

The earth's atmosphere in the case under consideration can be looked upon as a stratified medium [6], that is, it can be assumed that the velocity of sound propagation $a(z)$ as well as component velocities of wind W_x, W_y, W_z

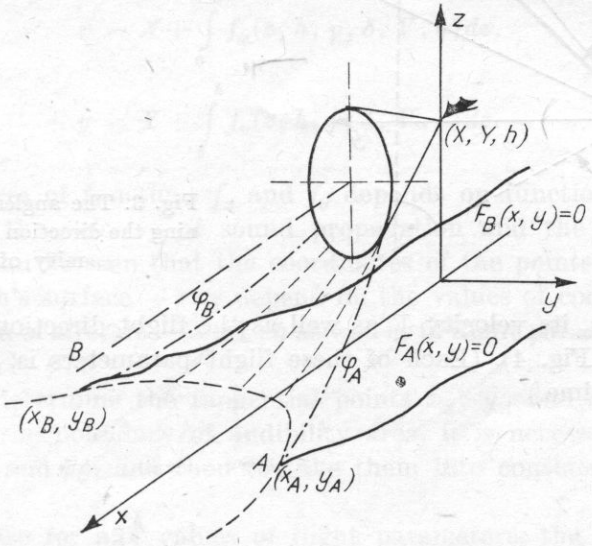

Fig. 2. Sets of the points of tangency of radii φ_A and φ_B with the earth's surface. Boundaries of audibility area: $F_A(x, y) = 0$, $F_B(x, y) = 0$

are functions of these heights. These parameters are decisive for the course of acoustic radii. If we assume that vertical component of wind $W_a = 0$, then the differential equation for radii takes the form [10]

$$\frac{dx}{dz} = -\cos\vartheta \frac{Ca^2 + W_x[1 - C(W_x + \tan\vartheta W_y)]}{a\sqrt{\cos^2\vartheta[1 - C(W_x + \tan\vartheta W_y)]^2 - C^2a^2}},$$
$$\frac{dy}{dz} = -\cos\vartheta \frac{Ca^2\tan\vartheta + W_y[1 - C(W_x + \tan\vartheta W_y)]}{a\sqrt{\cos^2\vartheta[1 - C(W_x + \tan\vartheta W_y)]^2 - C^2a^2}}, \quad (1)$$

where

$$C = \frac{\cos\theta}{a + \cos\theta(W_x + \tan\vartheta W_y)} \quad \text{for } z = h; \quad (2)$$

the angles ϑ and θ (Fig. 3) determine the direction of a radius in the proximity of the plane relative the coordinate system related to the earth.

The functions $W_x(z)$ and $W_y(z)$ can be determined with the aid of wind measurement at various heights. In a similar manner we determine the velocity of sound propagation $a(z)$.

The position of tangential points of radii φ_A and φ_B relative to earth's surface depends not only on the atmospheric conditions which were considered in equations (1) via the function a, W_x and W_y, but also on the aircraft position

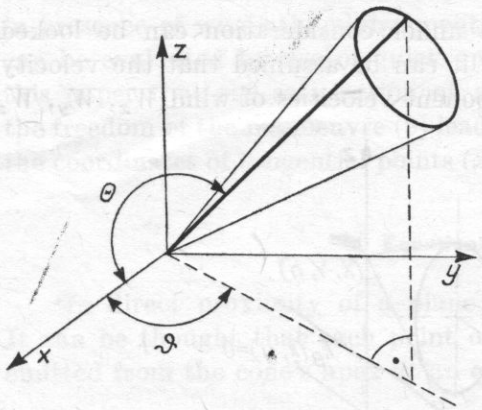

Fig. 3. The angles ϑ and θ determining the direction of ray in the proximity of aircraft

X, Y, h, (Fig. 2), its velocity V as well as the flight direction defined by the angles γ and δ (Fig. 4). (Each of these flight parameters is, in general case, the function of time.)

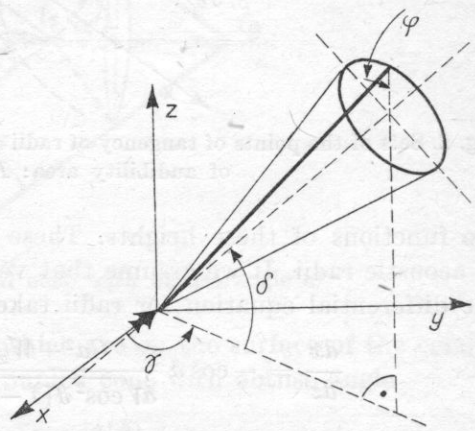

Fig. 4. The angles γ and δ determining the direction of flight

The dependence of the audibility area boundary on the flight parameters is obtained by the dependencies between the angles ϑ and θ (Fig. 3) as well as on the obtuse angle of the coupled cone α', the direction of its axis defined by the angles γ, δ and the position of the radius on the cone side. From trigonometric calculations we get

$$\vartheta = \gamma + \arctan\left\{\cot\alpha \frac{\sin\varphi}{\cos\delta}\right\}, \tag{3}$$

$$\cos\theta = \cos\gamma[\cos\delta\sin\alpha - \sin\delta\cos\alpha\cos\varphi] - \sin\gamma\cos\alpha\sin\varphi,$$

where

$$\alpha = \arcsin \frac{a(h)}{V}.$$

If we denote correspondingly the right members of equations (1) by f_x and f_y, then after substituting the relations (2) and (3) and integrating both members with respect to z, these equations take the form

$$x = X + \int_0^h f_x(z, h, \gamma, \delta, V, \varphi)\,dz,$$
$$y = Y + \int_0^h f_y(z, h, \gamma, \delta, V, \varphi)\,dz. \tag{1'}$$

(The apparent form of functions f_x and f_y depends on functions $a(z)$, $W_x(z)$, $W_y(z)$ describing the velocity of sound propagation and the wind velocity, respectively). It can be seen that the coordinates of the points of intersection of radii with earth's surface $-x, y$ depend on the values of coordinates determining the position of aircraft $-X, Y, h$ as well as of flight parameters: velocity $-V$ and direction $-\gamma, \delta$.

In order to determine the tangential points x_A, y_A and x_B, y_B (Fig. 2) which constitute the boundary of audibility area, it is necessary to find the value of angles φ_A and φ_B, and then to take them into consideration in equations (1').

In general case for any values of flight parameters, the magnitudes φ_A and φ_B cannot be described by an analytical formula, but it is only possible to point to a procedure which enables to find numerical values φ_A and φ_B (this case will be referred to as «general case»). It requires the use of computers.

The problem is considerably simplified when we make an assumption limiting the intervals of variability of flight parameters. Then the magnitudes φ_A and φ_B, thus also the coordinates of the tangential points, can be described by means of simple dependencies (the case will be referred to as «particular case»).

3. Determination of audibility area — general case

The tangency of a ray with the earth's surface means that the relations

$$\frac{dz}{dx} = 0, \qquad \frac{dz}{dy} = 0 \quad \text{for } z = 0$$

are satisfied.

From equations (1) it can be seen that this implies the equality

$$\cos\vartheta\,[1 - C(W_x(0) + \tan\vartheta\, W_y(0))] = Ca_0. \tag{4}$$

Taking into account (2) we have

$$\cos\vartheta = \frac{a_0}{a(h)}\cos\theta\left[1-\sin\vartheta\frac{W_x(h)-W_x(0)}{a_0}-\cos\vartheta\frac{W_y(h)-W_y(0)}{a_0}\right], \quad (5)$$

where a_0, $W_x(0)$, $W_y(0)$; $a(h)$, $W_x(h)$, $W_y(h)$ denote velocities of sound propagation and component wind velocities at the earth's surface $z = 0$ and at the height $z = h$, respectively. The angles ϑ and θ are described by equations (3).

Expression (5) is a transcedental equation with respect to φ whose solution are the values of angles φ_A and φ_B for which the rays are tangent to the earth's surface. This solution can be obtained with the aid of a computer. By substituting φ_A and φ_B in equations (1′) we get the coordinates of tangential points $x_A(t)$, $y_A(t)$ as well as $x_B(t)$, $y_B(t)$ (Fig. 2) as a time function. By the elimination of the parameter t we get the boundary of the audibility area of sound shock wave in the form of equations $F_A(x, y) = 0$ and $F(x, y) = 0$.

4. Determination of audibility area — particular case

The above-presented algorithm of the determination of the audibility area is rather complex. It can be seen that if the inequality

$$C|W_x+\tan\vartheta\cdot W_y| \ll 1 \quad \text{for } 0 \leqslant z \leqslant h \quad (6)$$

is satisfied, then this algorithm leads to comparatively simple analytical expressions. (The physical interpretation of this inequality will be given.)

Inequality (6) simplifies expression (2) to the form

$$C = \frac{\cos\theta}{a(h)}.$$

In view of (3) we get

$$C = \frac{1}{a(h)}\{\cos\gamma\,(\cos\delta\sin\alpha-\sin\delta\cos\alpha\cos\varphi)-\sin\gamma\cos\alpha\cos\varphi\}. \quad (7)$$

Equation (4) and inequality (6) imply that $\cos\vartheta = Ca_0$. From (3) and (7) we obtain the following equation with respect to φ:

$$\cos\left\{\gamma+\arctan\frac{\sin\varphi\cot\alpha}{\cos\delta}\right\} = \frac{a_0}{a(h)}\left[\cos\gamma(\cos\delta\sin\alpha-\sin\delta\cos\alpha\cos\varphi)-\sin\gamma\cos\alpha\sin\varphi\right]$$

The identical relation is obtained from (5) under the assumption that $W_x = 0$, $W_y = 0$. This means that in this case the value of the angle φ for

which the radii are tangent to the earth's surface do not depend on the γ. Hence it can be concluded that said equations can be reduced to the form

$$\cos\left\{\gamma+\arctan\frac{\sin\varphi\cot a}{\cos\delta}\right\}=\cos\{\gamma+\psi\},$$

where

$$\cos\psi=\pm\frac{a_0}{a(h)}(\cos\delta\sin a-\sin\delta\cos a\cos\varphi),$$

$$\sin\psi=\pm\frac{a_0}{a(h)}\cos a\sin\varphi;$$

from the identity $\cos^2\psi+\sin^2\psi=1$ we get

$$\cos\varphi=-\tan\delta\tan a-\frac{\sqrt{1-a^2(h)/a_0^2}}{\cos a\cos\delta}.$$

Substituting $\cos\varphi$ as well as $\sin\varphi=\pm\sqrt{1-\cos^2\varphi}$ into (7) we get the constant values C_A and C_B, from the relation $\cos\vartheta=Ca_0$ – the constants ϑ_A and ϑ_B. Next, to abbreviate the notation, we shall use the symbols $C_{A,B}$ and this will mean that we have to do either with the constant C_A or with the constant C_B (the same applies to the constants ϑ_A and ϑ_B as well as to the coordinates of the points of tangency x_A, x_B, y_A, y_B).

Equations (1′) can be re-written in the following form:

$$\begin{aligned}x_{A,B}&=X+\int_0^h\frac{C_{A,B}a^2+W_x}{a\sqrt{1-a^2/a_0^2}}\,dz,\\ y_{A,B}&=Y+\int_0^h\frac{\pm(a^2/a_0)\sqrt{1-C_{A,B}^2a_0^2}+W_y}{a\sqrt{1-a^2/a_0^2}}\,dz.\end{aligned}\tag{8}$$

Let us return to inequality (6) which is the starting point for the method in question. If we substitute (2) in this inequality, we get

$$\cos\theta\left\{\frac{W_x}{a}+\left(\frac{W_x}{a}\right)_h+\tan\vartheta\left[\frac{W_y}{a}+\left(\frac{W_y}{a}\right)_h\right]\right\}\ll 1.$$

Since the wind velocity is, in general considerably smaller than the velocity of sound propagation, this inequality will be satisfied if $|\vartheta|<\frac{1}{2}\pi$, which means that the following relation for the parameters γ, δ, V

$$\left|\gamma+\arctan\left\{\frac{\sqrt{V^2-a^2(h)}}{a(h)\cos\delta}\right\}\right|<\frac{1}{2}\pi\tag{9}$$

holds.

This inequality is satisfied, when the aircraft flight is very similar to the rectilinear flight, i.e. when turns in the horizontal plane – the angle γ, as well as in the vertical plane – the angle δ (Fig. 4), are not too acute. This means that in the case of ascent (upward flight) for which we have $\delta \to \frac{1}{2}\pi$ or of turn $\gamma \to \frac{1}{2}\pi$ we cannot use equations (8). On the other hand, if we assume that we have to do wit passenger aircraft, then from the viewpoint of the flying comfort it is necessary to dispense with such manoeuvres. Then, relations derived in this chapter can be utilized for planned flight channels or can be used as one of the prerequisites for country's regional planning under the assumption that flight channels are determined beforehand.

On the basis of results presented in [4] it can be assumed that the velocity of sound propagation is the linear function of altitude

$$a = a_0(1-\beta z) \quad \text{for } z < 12 \text{ km},$$

while the components of wind velocity can take the form of multinominals

$$W_x = \sum_{k=0}^{n} a_k^{(x)} z^k, \qquad W_y = \sum_{k=0}^{n} a_k^{(y)} z^k.$$

Substituting these magnitudes into equations (8) we get

$$x_{A,B} = X + C_{A,B} a_0 \sqrt{\frac{h(2-\beta h)}{\beta}} + \frac{1}{a_0 \beta} \sum_{k=0}^{n} \sum_{m=0}^{k} \frac{a_k^{(x)}}{\beta^k} \binom{k}{m} (-1)^m \int_1^{1-\beta h} \frac{\xi^m \, d\xi}{\sqrt{1-\xi^2}},$$

$$y_{A,B} = Y \pm \sqrt{1 - C_{A,B}^2 a_0^2} \sqrt{\frac{h(2-\beta h)}{\beta}} + \frac{1}{a_0 \beta} \sum_{k=0}^{n} \sum_{m=0}^{k} \frac{a_k^{(x)}}{\beta^k} \binom{k}{m} (-1)^m \int_1^{1-\beta h} \frac{\xi^m \, d\xi}{\sqrt{1-\xi^2}}. \tag{10}$$

If the weather is windless ($W_x = 0$, $W_y = 0$), then the coordinates of points which constitute the boundary of the audibility area of supersonic flight $x_A y_A$, $x_B y_B$, considering the mode of notation $x_{A,B}$, $y_{A,B}$, $C_{A,B}$ as explained above, take the form

$$x_{A,B} = X + C_{A,B} a_0 \sqrt{\frac{h(2-\beta h)}{\beta}}, \quad y_{A,B} = Y \pm \sqrt{1 - C_{A,B}^2} a_0^2 \sqrt{\frac{h(2-\beta h)}{\beta}}, \tag{11}$$

where X, Y, h denote the coordinates that determine the position of aircraft (Fig. 2), $C_{A,B}$ – the constant defined by (2), a_0 – the velocity of sound propagation at the earth's surface, β – the constant determining the changes of velocity of the sound propagation in the atmosphere.

5. Rectilinear flight

During the rectilinear flight on the constant height h, i.e. with $\delta = 0$, it is a good practice to choose the coordinate system so that $\gamma = 0$. In this case, in agreement with (7), we have $C = 1/V$.

Furthermore, if we assume that $W_x = 0$ and $W_y = 0$, then from equations (11) we get

$$x_{A,B} = \int V(t)\,dt + \frac{a_0}{V(t)}\sqrt{\frac{h(2-\beta h)}{\beta}}, \quad y_{A,B} = \pm\sqrt{1-\frac{a_0^2}{V^2(t)}}\sqrt{\frac{h(2-\beta h)}{\beta}}. \tag{12}$$

Hence, it can be seen that the audibility area of a supersonic flight is a belt with the axis of symmetry X (Fig. 2).

For the constant air speed we obtain the well-known formula for the width of this belt:

$$d = 2\sqrt{1-\frac{a_0^2}{V_0^2}}\sqrt{\frac{h(2-\beta h)}{\beta}}. \tag{13}$$

In paper [11] the results of numerical calculations of d are given.

From the above formulae it results that $d = 0$ if $V(t) = a_0$. This means that the supersonic flight is inaudible when air speed is smaller than the velocity of sound propagation at the earth's surface.

Let us assume that the initial flight stage is effected at a speed $V = a_0 + m_1 t$. Substituting $V(t)$ into (12) and eliminating t we get the equation that corresponds to the broken curves shown in Fig. 5:

$$x = \frac{a_0^2}{m_1}\left[\frac{1}{\sqrt{1-y^2/x^2}} - 1\right] + \frac{a_0^2}{2m_1}\left[\frac{1}{\sqrt{1-y^2/x^2}} - 1\right]^2 + \sqrt{x_0^2+y^2},$$

$$x_0 = \sqrt{\frac{h(2-\beta h)}{\beta}}.$$

It can be proved that the course of those curves depends on the satisfaction of the relation

$$M_1 \gtrless \frac{a_0^2}{x_0}.$$

Since the boundary of the audibility area of the flight is a set of the tangential points of radii to the earth's surface, which simultaneously confine the beam of rays that intersect the earth's surface. This implies that with accelerations $m_1 < a_0^2/x_0$ the shock wave will two times reach the shaded area in Fig. 5. This phenomenon of «double boom», caused by supersonic flight, is observed in practice [2, 5, 12].

If the transition to subsonic speed is effected with uniformly retarded motion $V(t) = V^* - m_2 t$, then the boundary of the audibility area is a curve (continuous line in Fig. 5):

$$x = x_0 + \frac{V^*}{m_2}\left[V^* - \frac{a_0}{\sqrt{1-y^2/x_0^2}}\right] - \frac{1}{2m_2}\left[V^* - \frac{a_0}{\sqrt{1-y^2/x^2}}\right]^2 + x_0\sqrt{1-\frac{y^2}{x_0^2}}.$$

6. Conclusions

The boundary of the audibility area of the shock wave caused by supersonic flight can — in general case (when the aircraft makes arbitrary manoeuvres) — be determined by means of the algorithm described in Section 3.

If the flight is similar to rectilinear one, then this area can be found with the aid of relations derived in Section 4.

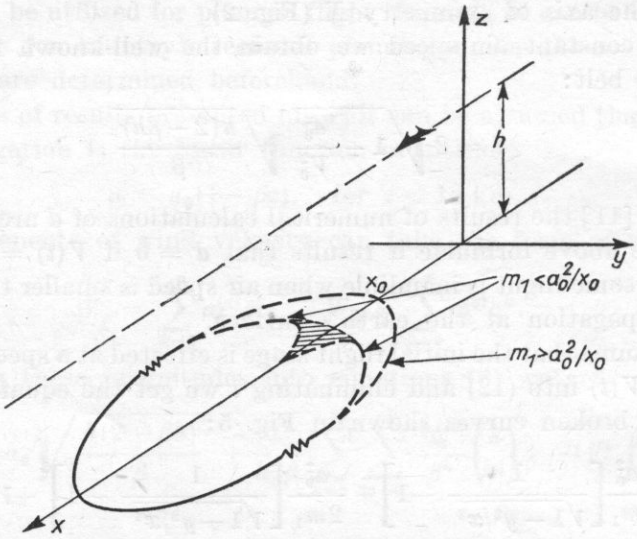

Fig. 5. The boundary of audibility area during the flight at a speed $V = a_0 + m_1 t$ (broken line) and a speed $V = V^* - m_2 t$ (continuous line).
Shaded area — the place of the occurrence of «double boom»

The reason and the mechanism of the so-called «double boom» are explained and the area of its occurrence is determined (Section 5).

The results presented can be helpful in regional planning to scale of macroregion and of the country.

References

[1] C. BARLETT, M. FRIEDMANN, *A method for calculating the effect of aircraft manoeuvres on sonic boom*, Jour. of Aircraft, 2, 5 (1965).

[2] A. BIESTEK, *Analysis and methods of the determination and propagation of sonic boom*, doctor's thesis [in Polish], Department of Mathem., Phys., Chem. of A. Mickiewicz University, Poznań 1973.

[3] J. EDWARDS, *Lateral extents of sonic boom carpets in real atmospheres*, Roya Aircraft Establishment, Tech. Mem. Aero., 1445, 1972.

[4] G. GROVES, *The structure of the atmosphere up to 150 kilometre*, Contemp. Phys. 14, 1 (1973).

[5] G. HAGLUND, E. KANE, *Flight test measurements and analysis of sonic boom phenomena near the shock wave extremity*, NASA CR-216, 1973.

[6] W. HAYES, H. RUNYAN, *Sonic-boom propagation through a stratified atmosphere*, JASA, 51, 2 (1972).

[7] D. HILTON, H. HENDERSON, *Measurements of sonic-boom overpressures from Apollo space vehicles*, JASA, **56**, 2 (1974).

[8] D. MAGLIERI, *Experiments on the effects of atmospheric refraction and airplane accelerations on sonic-boom groundpressure patterns*, NASA TN-3520,1966.

[9] D. LANSING, *Application of acoustic theory to prediction of sonic boom ground patterns from manoeuvering aircraft*, NASA TN D-1860, 1964.

[10] R. MAKAREWICZ, *Differential equations of rays in moving non-homogeneous medium* [in Polish], Archiwum Akustyki, **11**, 1 (1976).

[11] R. MAKAREWICZ, *Ergonomic analysis of manoeuvers leading to inaudibility of shock wave* [in Polish], Materials from the conference «Ergonomy in Aviation», Warszawa 1975.

[12] I. WANNER, *Bang Sonique. Théorie et expérimentation du phénomène de focalisation*, Association Technique Maritime et Aerotique, Session 1969.

[13] C. WARREN, *The propagation of sonic bangs in a non-homogeneous still atmosphere*, 4-th Congress Aeronautical Sciences, London 1965.

Received on 31st October 1975

ARCHIVES OF ACOUSTICS
1, 4, 269-298 (1977)

PROPERTIES OF ACOUSTIC BARRIERS IN A FIELD OF REFLECTED WAVES

STEFAN CZARNECKI, EWA KOTARBIŃSKA

Department of Aeroacoustics, Institute of Fundamental Technological Research of the Polish Academy of Sciences (Warszawa)

This paper deals with the effect of selected factors on the properties of acoustic barriers.

Most attention has been paid to the influence of reflected waves which diminish the effectiveness of a barrier for the area behind it.

The considerations were limited to interiors with an extended ceiling and for cases involving one or a few noise sources. Such conditions occur often in industrial halls and in urban areas. Under these circumstances the condition of equal energy density distribution is not fulfilled, so the reverberation theory is not valid. Hence, the mirror method was used which constitutes an extension of the image source method by the mirror representation of all diffracting and absorbing surfaces.

Analytical relations were obtained, which permit the calculation of the effect of the reflected waves in decreasing the insertion loss of a barrier. Two established criteria, spatial and energetic were used. The theoretical analysis was confirmed by experimental results.

1. Introduction

The effectiveness of acoustic barriers depends on many factors which may be divided into three basic groups:

– the geometry of the system: sound source–barrier–observer,

– the properties of barrier (insulating properties, geometric diamensions, shape),

– the surrounding acoustical conditions (free field, reflected wave field, reverberant field).

The factors mentioned above are mutually interrelated. Hence a full analysis of barrier performance requires examination of the problem as a multi-parameter one.

Up to now, most attention has been paid to the problem of the geometry of the system comprising the source, barrier and observer. The influence of the

surrounding acoustical conditions was not deeply investigated although it has a fundamental influence on the sound intensity level in the area behind the barrier.

The main aim of this paper is to examine the influence of the surrounding acoustical conditions in the case where the system source–barrier–observer is situated in the reflected wave field.

2. The effectiveness of a barrier

The effectiveness of a barrier is represented by the insertion loss IL, defined as the difference of the mean squared sound pressure levels at a certain point of an acoustic field, in the absence of a barrier and after its installation.

Denoting the sound pressure levels L and the average values of the squared pressures $\overline{p}^2$ by means of the subscript w in the absence of the barrier and by the subscript b with the barrier, we obtain from the definition the basic expression for the effectiveness of a barrier, given by the insertion loss

$$IL = L_w - L_b = 10 \log \frac{\overline{p}_w^2}{\overline{p}_b^2}. \tag{1}$$

In the simplest case, $\overline{p}_w^2$ represents the direct wave and $\overline{p}_b^2$ the wave diffracted at the barrier edge.

In the general case, a wave generated by a source S may reach the observer in different ways which we denote by the following subscripts for the symbols $\overline{p}^2$ and IL:

d – for the path of a wave diffracted at the upper of the barrier edge,
e – for the path of a wave diffracted at the side edges of the barrier,
i – for the wave propagated through the barrier,
r – for the waves reflected from the boundaries of the room,
o – for a direct wave without the barrier.

Thus we may write, for waves reaching an observer behind a barrier:

– without barrier

$$\overline{p}_w^2 = \overline{p}_0^2 + \overline{p}_r^2, \tag{2}$$

– with barrier

$$\overline{p}_0^2 = \overline{p}_d^2 + \overline{p}_e^2 + \overline{p}_i^2 + \overline{p}_{rb}^2, \tag{3}$$

where the subscript rb refers to waves reflected with the barrier installed.

Accounting for all paths of acoustic wave transmission simultaneously, expression (1) for the barrier effectiveness can be determined by the relationship

$$IL_{deir} = 10 \log \frac{\overline{p}_0^2 + \overline{p}_r^2}{\overline{p}_d^2 + \overline{p}_e^2 + \overline{p}_i^2 + \overline{p}_{rb}^2}. \tag{4}$$

3. Barrier action in a free field

Accurate analysis of the acoustic barrier action requires a quite complex mathematical description of the acoustic wave diffraction phenomenon. However, the studies of MAEKAWA [5, 6], RATHE [10] and others have created a simplified theory leading to practically useful simple formulae for the effectiveness of the barrier in a free field. These formulae differ slightly depending on the assumptions of the restrictions but they can be written in the general form

$$IL_d = 10 \log(C + qN), \tag{5}$$

where, according to Maekawa [5, 7] $C = 3$ and $q = 20$, and according to Rathe $C = 0$ and $q = 20$, assuming $N > 1$. Wells [13] derived a formula in which $C = 1$ and $q = 10$ for $N > 0$.

Differences in the value of C are significant only for small values of N. The difference in the values of q alter the value of IL by 3 dB.

In order to simplify calculations, the following formulae will be used:

$$IL_d = 10 \log M, \tag{6}$$

$$M = \begin{cases} 20N & \text{for } N \geqslant 1, \\ 20N + 3 & \text{for } 0 > N > 1. \end{cases} \tag{6a}$$

In these formulae N is the Fresnel number,

$$N = 2\delta/\lambda, \tag{7}$$

where λ is the wavelength and δ, according to the notation in Fig. 1a, represents the difference between the path lengths of the diffracted and the direct waves:

$$\begin{aligned} \delta &= R_1 + R_2 - (r_1 + r_2) \\ &= h_{ef}\left[\left(\frac{1}{\sin\varphi_1} + \frac{1}{\sin\varphi_2}\right) - \left(\frac{1}{\tan\varphi_1} + \frac{1}{\tan\varphi_2}\right)\right], \end{aligned} \tag{8}$$

where h_{ef} is the effective barrier height obtained by plotting a line from the upper barrier edge perpendicularly to the line connecting the point S of source with the point O of the observer.

In free field conditions the effectiveness of the barrier depends on two factors:

a. the geometry of the system source–barrier–observer,

b. the properties of the barrier itself.

a. *The geometry of the system source–barrier–observer.* Fig. 1 shows that in the general case of an asymmetric configuration (Fig. 1a) the estimation of the distances R_1, R_2, r_1, r_2 or h_{ef}, φ_1 and φ_2, based on the geometric positions of the source, the observer and the barrier, leads to tedious calculations. Much simpler is the symmetrical system (Fig. 1b), in which $R_1 = R_2 = R$, $r_1 = r_2 = r$, $\varphi_1 = \varphi_2 = \psi/2 = \varphi$ where ψ is the angle of diffraction.

Assuming, after Rathe, that $C = 0$ and $q = 20$ we can write the expression for the effectiveness of the barrier,

$$IL_d = 10 \log \frac{\overline{p}_0^2}{\overline{p}_d^2} = 10 \log 20N = 10 \log \frac{80(R-r)}{\lambda} = 10 \log \frac{160h}{\lambda} f(\psi), \tag{9}$$

where $f(\psi)$ is a function of the diffraction angle given by the relation

$$f(\psi) = \frac{\sin^2(\psi/4)}{\sin(\psi/2)} = \frac{1}{2} \tan \frac{\psi}{4} = \frac{1}{2} \tan \frac{\varphi}{2}. \tag{10}$$

Formula (9) does not take into account the effect of spherical wave propagation which can be expressed by the coefficient k:

$$k = \left(\frac{R}{r}\right)^2 = \frac{1}{\cos^2(\psi/2)}. \tag{11}$$

This coefficient has an obvious meaning for short distances between the sound source and the observer, a situation that occurs very often in industrial

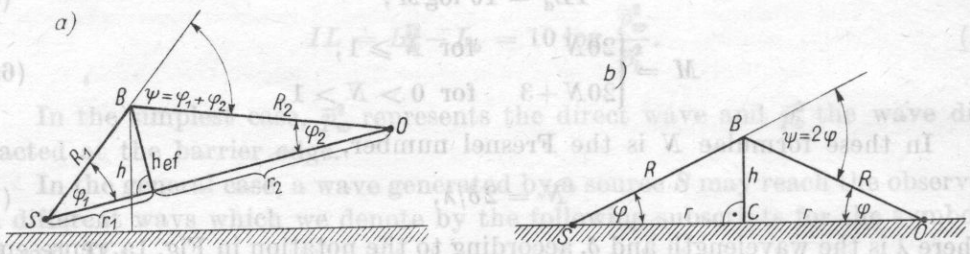

Fig. 1. The system source–barrier–observer
a) asymmetrical, b) symmetrical

conditions. It may be neglected for large distances, e.g. in the consideration of urban areas.

However, the relationship for the coefficient k represents an approximation, since the wave can be treated as a spherical one in the source–barrier region only. From the barrier to the observer it is more accurate to assume cylindrical waves.

In view of equation (11), the expression for IL_d becomes

$$IL_d = 10 \log \frac{160hf(\psi)k}{\lambda} = 10 \log \frac{80h}{\lambda} \frac{\tan(\psi/4)}{\cos^2(\psi/2)}, \tag{12}$$

which implies the formula

$$20N = \frac{\overline{p}_0^2}{\overline{p}_d^2} = \frac{20 \cdot 4(R-r)}{\lambda} \left(\frac{R}{r}\right)^2$$

$$= \frac{1}{\lambda} \frac{20 \cdot 8h}{\sin(\psi/2)} \frac{\sin^2(\psi/4)}{\cos^2(\psi/2)} = \frac{20 \cdot 4h}{\lambda} \frac{\tan(\psi/4)}{\cos^2(\psi/2)}. \tag{13}$$

Fig. 2 shows IL_d as a function of the diffraction angle for $h/\lambda = 1$ and $h/\lambda = 10$. Curves a have been calculated with the formula usually found in the references [7, 10], where this formula is without the coefficient k. Curves b were calculated according to (12).

In order to compare the analytical results, the additional curves c were plotted in Fig. 2 for identical ratios of h_{ef}/λ, obtained from the diagram of MAEKAWA [7] using the diffraction angle as an independent variable. Similar curves are also obtained by an identical treatment of the curves of KURZE [4].

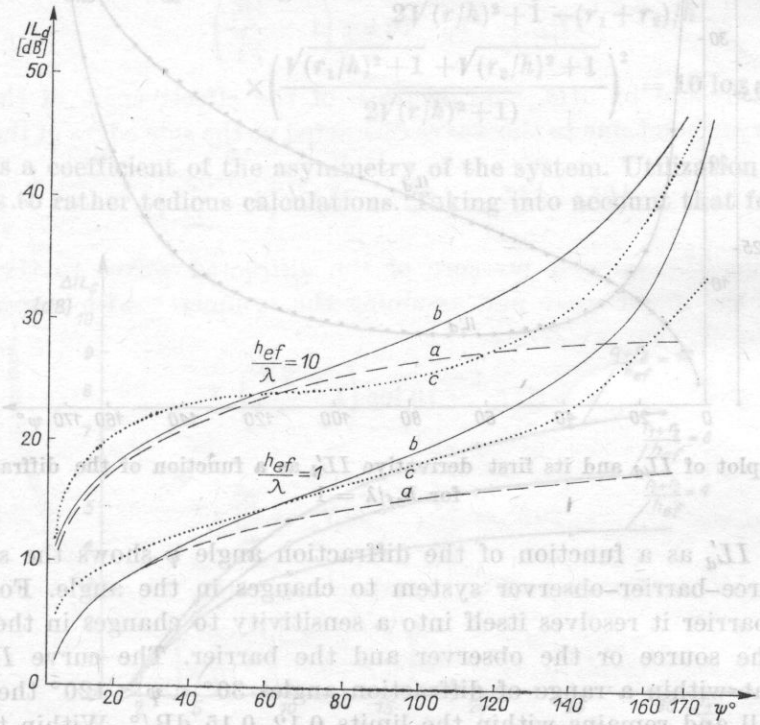

Fig. 2. Relationship between IL_d and the diffraction angle ψ for symmetrical system for $h_{ef}/\lambda = 1$ and $h_{ef}/\lambda = 10$

a) curve calculated from formula (10) without correction for the sphericity of the waves, *b*) curve calculated from formula (12) taking into account a correction for the sphericity of the waves, *c*) curve obtained by replotting of the graph of MAEKAWA [7]

The curves b and c show an increase compared to curve a of the IL_d for high values of the diffraction angle ψ, if the correction for sphericity of waves has a greater significance. It confirms the usefulnes of introducing this correction, although differences between curves b and c indicate that further analysis is required.

In order to analyse more precisely the changes of IL_d versus diffraction angle the first derivative of IL_d has been calculated and plotted in Fig. 3,

$$IL'_d = \frac{d(IL_d)}{d\psi}. \tag{14}$$

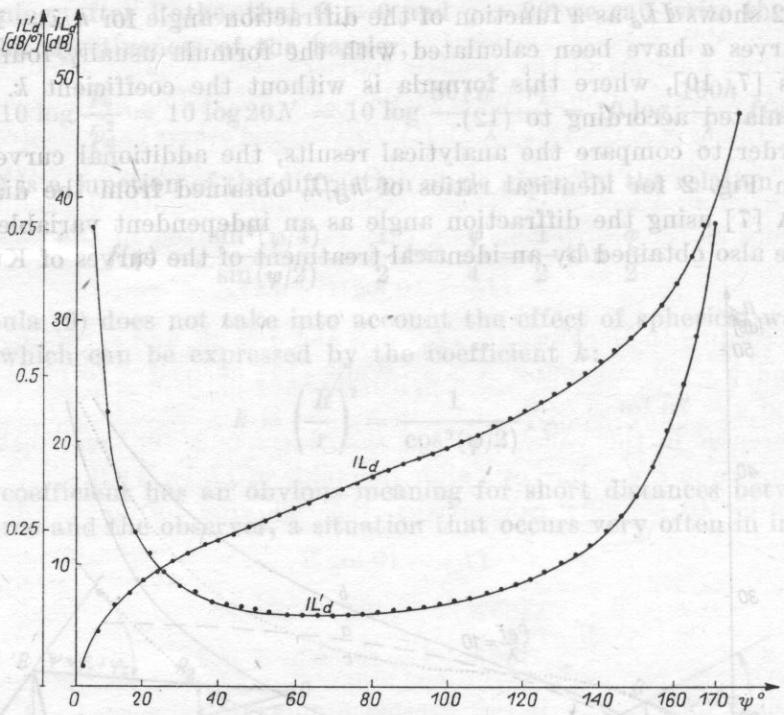

Fig. 3. The plot of IL_d and its first derivative IL'_d as a function of the diffraction angle for $h_{ef}/\lambda = 1$

The curve IL'_d as a function of the diffraction angle ψ shows the sensitivity of the source–barrier–observer system to changes in the angle. For a fixed height of barrier it resolves itself into a sensitivity to changes in the distance between the source or the observer and the barrier. The curve $IL_d = f(\psi)$ implies that within a range of diffraction angles $30° < \psi < 120°$ the value of IL'_d is small and remains within the limits 0.12 - 0.15 dB/°. Within this range of angles, the system shows little sensitivity to changes in the diffraction angle.

This permits the introduction of a „criterion of 30°" which, taking into account the economical arguments, determines the optimal value of the diffraction angle for large distances between the sound source and the observer compared with the effective height of the barrier. This criterion leads to a practical conclusion which can be applied in town planning acoustics.

For small distances between the source and the observer to the barrier a criterion of 120° can be introduced. In situation where the diffraction angle ψ is about 120° it is useful to make this angle as large as possible, because it very greatly increases the effectiveness of the barrier. This conclusion may be highly important in the design of industrial interiors and offices.

From these considerations an additional problem arises in the asymmetry of the arrangement. Relatively small errors should be expected when an asym-

metrical arrangement (Fig. 1a), which is inconvenient for analytical purposes, is transformed into a more convenient symmetrical one (fig. 1b) within a range of 30°-120° for the diffraction angle.

The difference ΔIL_s between IL_{dns} for an asymmetric arrangement and IL_{ds} for a symmetric one, assuming that the distance between the source and the observer is fixed, i.e. $r_1+r_2 = 2r = \text{const}$, may be calculated from the relation

$$\Delta IL_s = IL_{dns} - IL_{ds} = 10\log \frac{\sqrt{(r_1/h)^2+1} + \sqrt{(r_2/h)^2+1} - (r_1+r_2)/h}{2\sqrt{(r/h)^2+1} - (r_1+r_2)/h} \times$$

$$\times \left(\frac{\sqrt{(r_1/h)^2+1} + \sqrt{(r_2/h)^2+1}}{2\sqrt{(r/h)^2+1)}} \right)^2 = 10 \log \varepsilon, \quad (15)$$

where ε is a coefficient of the asymmetry of the system. Utilization of formula (15) leads to rather tedious calculations. Taking into account that for practical

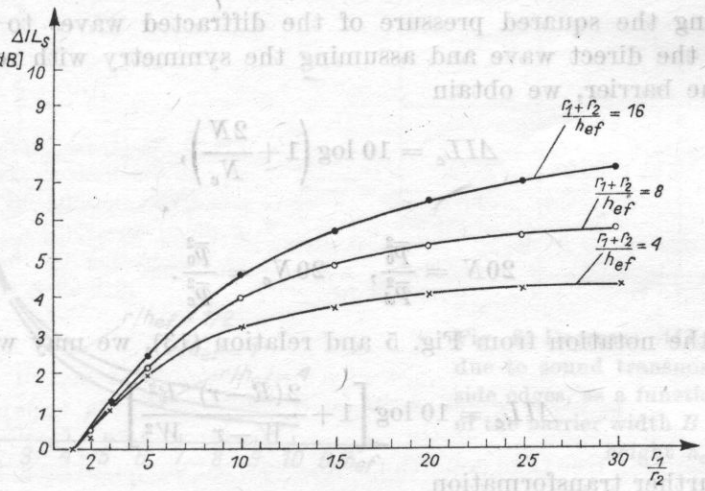

Fig. 4. Corrections ΔIL_s resulting from transformation of an asymmetrical arrangement to a symmetrical one as a function of the asymmetry r_2/r_1 or r_1/r_2

purposes the relation $\Delta IL_s = f(r_2/r_1)$ or $\Delta IL_s = f(r_1/r_2)$ is more convenient, it has been calculated for several values of parameter $(r_1+r_2)/h_{ef}$ and presented in Fig. 4. From these relations it results that, as expected, even for high values of r_1/r_2 or r_2/r_1 the error caused by the transformation from an asymmetric arrangement into a symmetric one is not high and can be included as the correction according to Fig. 4.

b. *Parameters of the barrier.* The width of the barrier and its insulating properties for airborne sounds will be examined as the parameters of the barrier which may cause a reduction in its resultant effectiveness.

In order to consider the influence of the barrier width on IL_d let us denote by $\overline{p}_e^2$ the mean squared sound pressure of the wave arriving at the observer in consequence of diffraction at the edge of one side of the barrier. Since the waves are diffracted at two side edges of a barrier, we can write

$$IL_{de} = 10 \log \frac{\overline{p}_0^2}{\overline{p}_d^2 + 2\overline{p}_e^2} = 10 \log \frac{\overline{p}_0^2/\overline{p}_d^2}{1 + 2\overline{p}_e^2/\overline{p}_d^2}. \tag{16}$$

With expression (9) we get

$$IL_{de} = IL_d - 10 \log \left(1 + \frac{2\overline{p}_e^2}{\overline{p}_d^2}\right). \tag{17}$$

Let us denote by ΔIL_e the decrease of the effectiveness of the barrier at the observer point due to the waves diffracted at the side edges of the barrier:

$$\Delta IL_e = IL_d - IL_{de} = 10 \log \left(1 + \frac{2\overline{p}_e^2}{\overline{p}_d^2}\right). \tag{18}$$

Referring the squared pressure of the diffracted waves to the squared pressure of the direct wave and assuming the symmetry with respect to the width of the barrier, we obtain

$$\Delta IL_e = 10 \log \left(1 + \frac{2N}{N_e}\right), \tag{19}$$

where

$$20N = \frac{\overline{p}_0^2}{\overline{p}_d^2}, \qquad 20N_e = \frac{\overline{p}_0^2}{\overline{p}_e^2}. \tag{20}$$

Using the notation from Fig. 5 and relation (13), we may write

$$\Delta IL_e = 10 \log \left[1 + \frac{2(R-r)}{W-r} \frac{R^2}{W^2}\right] \tag{21}$$

and after further transformation

$$\Delta IL_e = 10 \log \left\{1 + \frac{2\left(\sqrt{r^2 + h_{ef}^2} - r\right)(r^2 + h_{ef}^2)}{\left[\sqrt{r^2 + (B/2)^2} - r\right][r^2 + (B/2)^2]}\right\}. \tag{22}$$

The relationship of ΔIL_e as a function of the ratio of the barrier width B to its effective height h_{ef}, with r/h_{ef} as a parameter, is shown in Fig. 6. This relationship enables to choose the width of the barrier, when a given decrease in its effectiveness is admitted.

In a similar way we can consider the decrease of barrier effectiveness due to the limited insulating properties of the barrier expressed by the insertion loss IL_i,

$$IL_i = 10 \log \frac{\overline{p}_0^2}{\overline{p}_i^2} = 10 \log \frac{1}{\tau}, \tag{23}$$

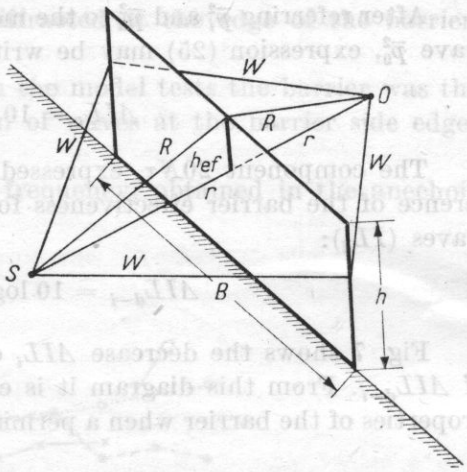

Fig. 5. The system source–barrier–observer in case of a limited barrier width B

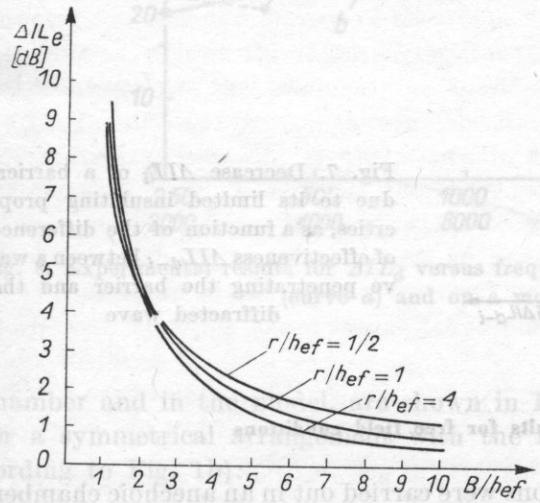

Fig. 6. Decrease ΔIL_e of a barrier, due to sound transmission along its side edges, as a function of the ratio of the barrier width B to its effective height h_{ef}

where $\overline{p}_i^2$ is the mean squared sound pressure of a wave penetrating the barrier, and τ is the transmission coefficient of the barrier.

The effectiveness of a barrier in the case of the joint action of diffracted waves and waves penetrating the barrier is then

$$IL_{di} = 10 \log \frac{\overline{p}_0^2}{\overline{p}_d^2 + \overline{p}_i^2} = 10 \log \frac{\overline{p}_0^2/\overline{p}_d^2}{1 + \overline{p}_i^2/\overline{p}_d^2} = IL_d - 10 \log \left(1 + \frac{\overline{p}_i^2}{\overline{p}_d^2}\right). \quad (24)$$

Hence, for the decrease ΔIL_i, caused by the part of the energy which penetrates through the barrier, we get

$$\Delta IL_i = IL_d - IL_{di} = 10 \log \left(1 + \frac{\overline{p}_i^2}{\overline{p}_d^2}\right). \quad (25)$$

After referring $\overline{p}_i^2$ and $\overline{p}_d^2$ to the mean squared sound pressure of the incident wave $\overline{p}_0^2$, expression (25) may be written in the form

$$\Delta IL_i = 10 \log(1+20N\tau). \tag{26}$$

The component $20N\tau$, expressed in logarithmic scale, represents the difference of the barrier effectiveness for penetrating waves (IL_i) and diffracted waves (IL_d):

$$\Delta IL_{d-i} = 10 \log 20N\tau = IL_d - IL_i. \tag{27}$$

Fig. 7 shows the decrease ΔIL_i of the barrier effectiveness as a function of ΔIL_{d-i}. From this diagram it is easy to determine the required insulating properties of the barrier when a permissible decrease of effectiveness is assumed.

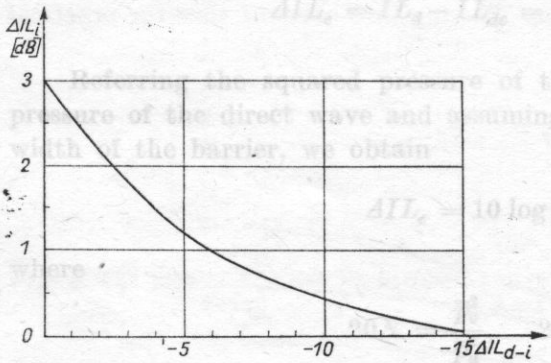

Fig. 7. Decrease ΔIL_i of a barrier, due to its limited insulating properties, as a function of the difference of effectiveness ΔIL_{d-i} between a wave penetrating the barrier and the diffracted wave

3. Experimental results for free field conditions

Experiments in free field conditions were carried out in an anechoic chamber over a frequency range of 250 Hz - 2000 Hz, and in an anechoic model with dimensions $83 \times 110 \times 150$ cm in a scale of 1 : 8, i.e. for a frequency range 2000 Hz - 16000 Hz.

The aim of the investigations was to check the agreement of the experimental results with the analytical ones and to assess the usefulness of model tests for further experiments involving a field of reflected waves.

The sound sources used were: loudspeaker of 14 cm diameter for tests in the anechoic chamber and 8.3 cm for the model tests. The irregularity of the directional characteristics of the loudspeakers was ± 3 dB in the frequency ranges of the experiments. A 1/2″ microphone was used in the anechoic chamber and 1/8″ microphone for model experiments.

Third octave band noise was used as a signal. The barrier used was partially reflecting, with transmission properties such that the energy penetrating the

barrier was at least 10 dB below that diffracted at the edge of the barrier, i.e. $IL_i - IL_d > 10$ dB.

Both in the anechoic chamber and in the model tests the barrier was the width of the room so that the diffraction of waves at the barrier side edges could be neglected.

Experimental results for IL_d versus frequency, obtained in the anechoic

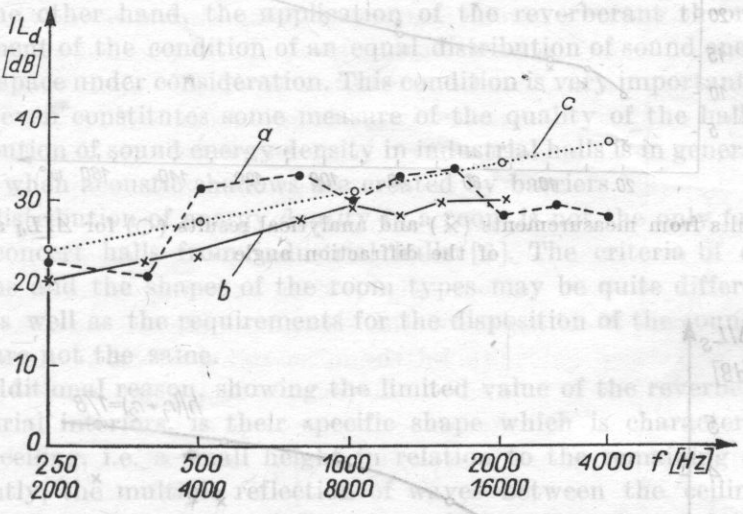

Fig. 8. Experimental results for ΔIL_d versus frequency, obtained in an anechoic chamber (curve *a*) and on a model (curve *b*)

chamber and in the model, are shown in Fig. 8. These results were obtained for a symmetrical arrangement with the following parameters (notation according to Fig. 1b):

$$h_{ef} = 20 \text{ cm}, \quad \psi = 60°.$$

The obtained results show good agreement and have confirmed the validity of the model for further investigations.

The results for IL versus the diffraction angle, obtained in the anechoic chamber for $h_{ef}/\lambda = 1.18$, are shown in Fig. 9.

The results are in conformity with the analytical curve and confirm the necessity of introducing a coefficient k for the sphericity of the waves at high values of the diffraction angle.

Results for the correction ΔIL_s, arising from an asymmetric arrangement with $h/(r_1 + r_2) = \frac{1}{8}$ as the parameter, are given in Fig. 10.

According to the analytical results, the values of the corrections ΔIL_s, for the parameter values mentioned above, do not exceed 4.5 dB.

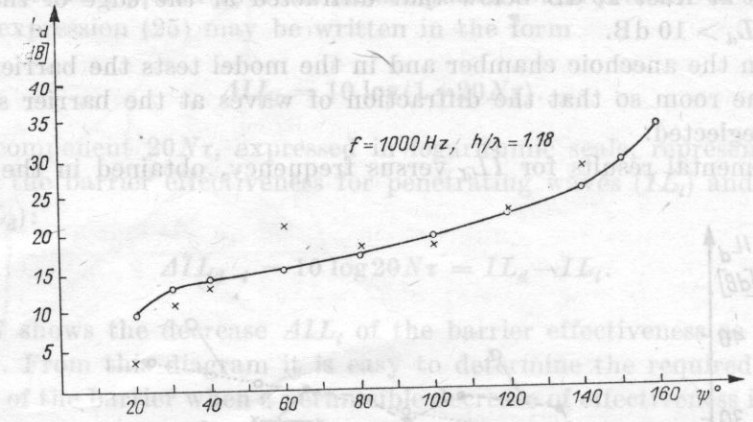

Fig. 9. Results from measurements (×) and analytical results (○) for ΔIL_d as a function of the diffraction angle

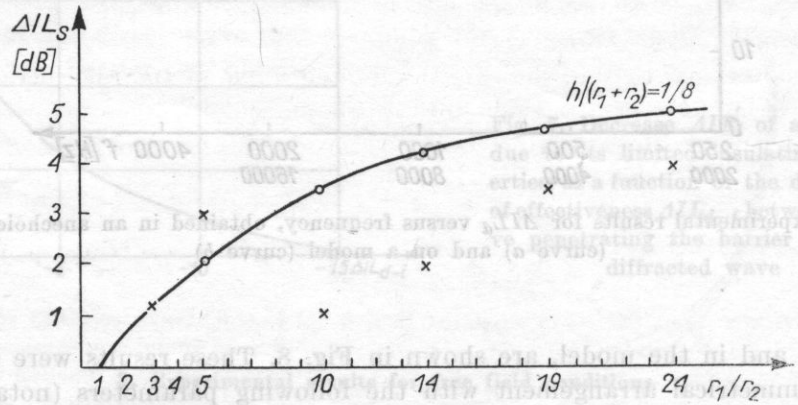

Fig. 10. Measured results for the correction ΔIL_s as a function of the asymmetry r_1/r_2 of the system

4. Barrier action in a field of reflected waves

When an infinitely wide barrier, which has infinitely high insulating properties, is placed in a field of reflected wave, then its effectiveness is given by formula (4):

$$IL_{dr} = 10 \log \frac{\overline{p}_0^2 + \overline{p}_r^2}{\overline{p}_d^2 + \overline{p}_{rb}^2} = 10 \log \frac{1 + \overline{p}_r^2/\overline{p}_0^2}{\overline{p}_d^2/\overline{p}_0^2 + \overline{p}_{rb}^2/\overline{p}_0^2}. \tag{28}$$

Formula (28) implies that if the observer is situated at the place where the energy of the reflected wave dominates the direct wave ($\overline{p}_r^2 > \overline{p}_0^2$), then the effectiveness of the barrier is very low ($IL_{dr} \cong 0$).

The influence of reflected waves in decreasing the effectiveness of barriers is usually discussed in terms of the reverberant theory of rooms. This theory leads to the conclusion that to obtain a high effectiveness of the barrier the reverberation time of the interior must be low [8]. It requires the use of the great quantity of absorbing material which is often expensive and difficult from a practical point of view. This is the reason why acoustic barriers are not very popular in practice.

On the other hand, the application of the reverberant theory demands the fulfilment of the condition of an equal distribution of sound energy density inside the space under consideration. This condition is very important for concert halls and even constitutes some measure of the quality of the hall. However, the distribution of sound energy density in industrial halls is in general irregular, especially when acoustic shadows are created by barriers.

The distribution of energy density in a room is not the only factor distinguishing concert halls from industrial halls [2]. The criteria of quality, the proportions and the shapes of the room types may be quite different or even opposite as well as the requirements for the disposition of the sound absorbing material are not the same.

An additional reason, showing the limited value of the reverberant theory for industrial interiors, is their specific shape which is characterized by an extended ceiling, i.e. a small height in relation to the remaining dimensions. Consequently, the multiple reflection of waves between the ceiling and the floor primarily decides the overall energy of the reflected waves.

Then as in urban areas a constant drop of the acoustic pressure level by 3 dB with doubling the distance takes place, without the occurrence of a critical distance [2, 12].

In consequence, the concept of a diffuse field will be replaced in the present paper by the a concept of a reflected wave field and, instead of the reverberant theory, the mirror method which constitutes an extension of the image source method will be used.

5. The mirror method

The image source method is used mainly as a qualitative means of imaging the reflected wave field by means of additional sound sources. This method has had a wide didactic application, but it can now be used as an analytical method [9] due to computer developments.

By the mirrorlike reproduction of the elements in the room (barriers, absorbing surfaces), the image source method may be extended into a method which we will call the mirror method. This method will be treated as an analytical method for calculating the sound intensity at any point of an acoustic field, taking into account the effect of the barrier and the absorbing surfaces.

For simplification, the analysis will be limited to rooms with an extended ceiling, which is, in general, very often the case in industrial halls. The problem thereby resolves itself into an analysis of the acoustic conditions in a room with two parallel reflecting surfaces and corresponds to the situation where image sources are arranged in only one axis.

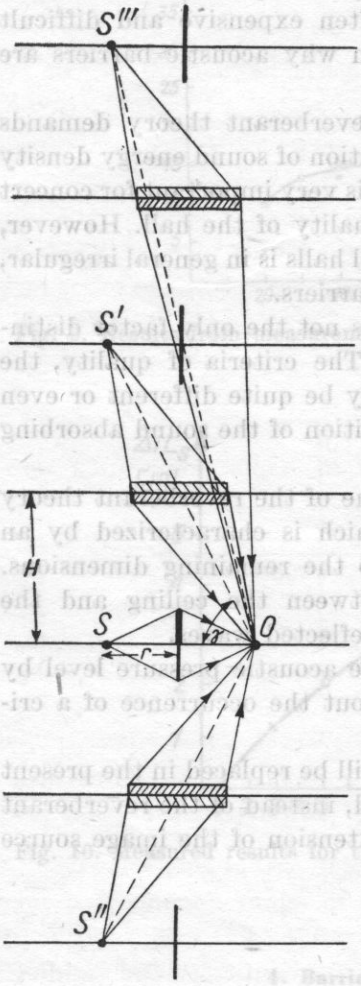

Let us assume that there is in the room only one source generating a spherical wave. The image sources will also radiate spherical waves. The acoustic power of the image sources will decrease respectively, being multiplied by the coefficient of reflection β, raised to a power corresponding to the number of times the wave has been reflected.

Assuming that the source is placed on the floor (Fig. 11), the following expression is obtained for the resulting reflected wave sound intensity for the noise signal at an observation point also on the floor, at a distance r from the source:

$$I_r \cong \frac{P}{\Psi} = \left[\beta + \frac{(1+\beta)^2}{(2H)^2} \sum_{i=1}^{\infty} \frac{\beta^{2i-1}}{i}\right]; \qquad (29)$$

H is the room height, P – the acoustic power of the source, and $\Psi < 2\pi$ – the solid angle for the image sources.

The effect of the reflected waves reaching the space behind the barrier can be reduced (i.e. the propagation of waves produced by the image sources) can be decreased by the following two methods:

Fig. 11. The principle of the mirror method

a. the choice of the height, shape and situation of the barrier;

b. a reduction of the coefficient of reflection of the surfaces situated above the barrier by fastening into the ceiling an absorbing band of suitable width.

The proper application of both methods can be analysed graphically by extending the method of image sources and by the mirrorlike reproduction of the barrier and absorbing bands, to produce image barriers and image absor-

bing bands. The waves produced by the image sources will arrive at the observation point without diffraction only when there are no image elements in their paths.

An analysis of the paths of rays representing the waves propagated from the image sources (Fig. 11) suggests the idea of treating the absorbing bands as band-barriers which limit the propagation of the waves generated by the image sources. This interpretation could be used for analytical purposes and would lead to uniform method of accounting for the effect of the barriers and the absorbing bands, based on the phenomenon of diffraction.

The action of the edges of the absorbing bands corresponds with the physical phenomenon of the scattering of acoustic energy in the form of the so-called edge effect, similar to the phenomenon of diffraction at an edge. This partially justifies the idea of band–barriers although a more detailed theoretical analysis is still required.

In the present paper the development of the band-barriers method as an analytical method has two aims:

— the initial evaluation of whether the method leads to simple mathematical relationships allowing the action of the absorbing bands and the barriers to be considered jointly and

— the checking of the agreement between the experimental and the analytical results obtained from the expressions based on the band-barrier concept.

Regarding the concept of band-barriers, the absorbing bands may be treated as a set of two barriers with an effective height related to the width of the absorbing band. The length of the band corresponds to the width of the barrier and the reflection coefficient β_a of the band material corresponds to the transmission coefficient τ of the barrier.

From Fig. 12 it can be easily seen that regions near the barrier are protected most effectively by the absorbing bands and this area expands for waves produced by the higher order image sources.

However, an area far behind the barrier is best protected against reflected waves by an image barrier, since near the barrier the image barrier limits only the propagation of those waves that are generated by lower order image sources. Also, with increasing distance, the number of image sources that are screened increases.

The effects of the image barriers and absorbing bands complement each other and their joint action provides a substantial limitation of the effect of reflected waves on the barrier *IL*.

The mirror method described above leads to more economical solutions than the statistical method. For industrial halls with extended ceilings and only a few noise sources it is possible to obtain a given reduction of reflected waves in a chosen region behind the barrier using much smaller quantities of sound absorbing material.

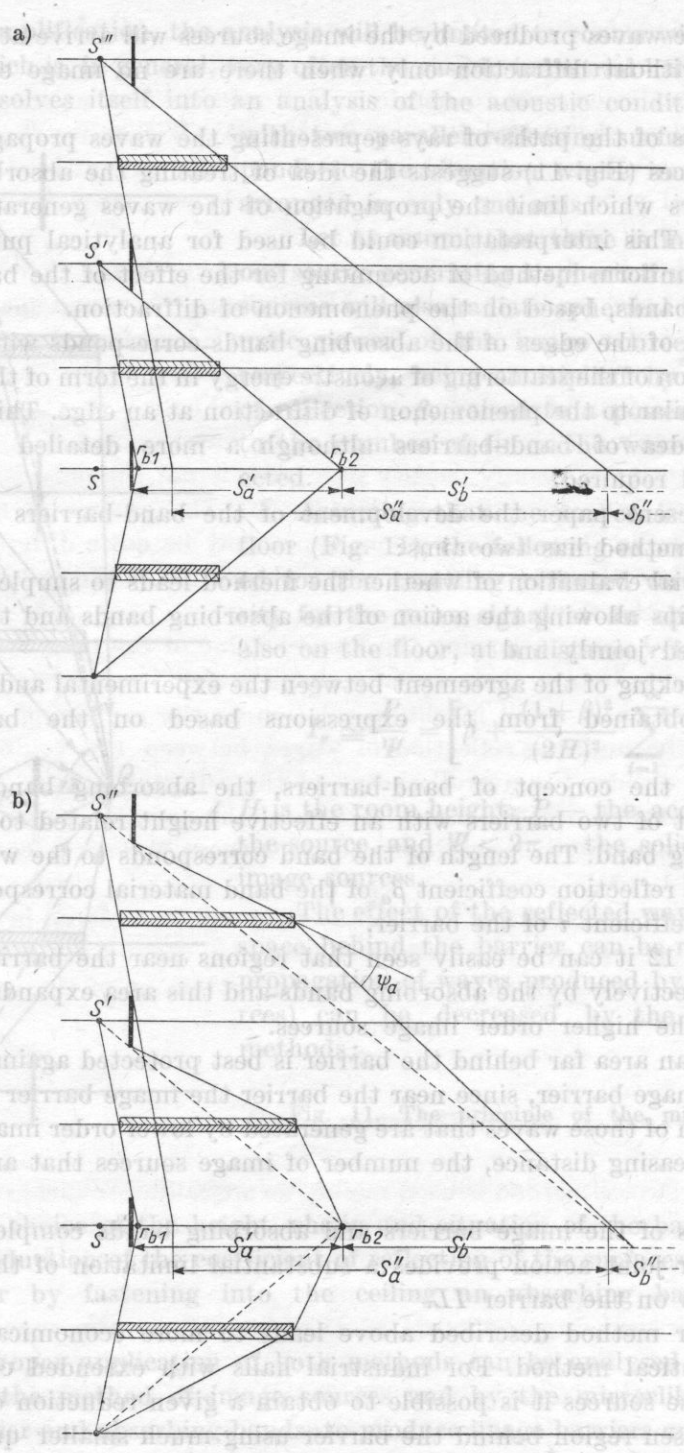

Fig. 12. Choice of the width of the absorbing bands using a geometrical method

6. Calculation of the IL_d in a field of reflected waves for the joint action of barriers and absorbing bands

In order to select the parameters of the barriers and absorbing bands giving jointly a sufficiently high (for an assumed criterion) limitation of reflected waves propagation (which reduces the effectiveness of the barriers), let us introduce the following symbols for the averaged values of the squared acoustic pressures at the observer point:

$\overline{p}_0^2$ – for the direct wave without the barrier,

$\overline{p}_d^2$ – for the wave diffracted at the barrier,

$\overline{p}_r^2$ – for the reflected waves (originating from the image sources) without the barrier and absorbing band,

$\overline{p}_{ra}^2$ – for the reflected waves limited by the action of the absorbing bands,

$\overline{p}_{rb}^2$ – for the reflected waves limited by the image barriers,

$\overline{p}_{rab}^2$ – for the reflected waves limited by the joint action of the absorbing bands and image barriers.

The effectiveness of the barriers in a field of reflected waves can be given as

$$IL_r = 10 \log \frac{\overline{p}_0^2 + \sum_{i=1}^{\infty} \overline{p}_{rai}^2}{\overline{p}_d^2 + \sum_{i=1}^{\infty} \overline{p}_{rabi}^2}. \tag{30}$$

For simplification let us consider separately the effect of image barriers which create an acoustical shadow for distances $r > r_{b2}$ and $r < r_{b1}$ behind the barrier and the effect of absorbing bands which create a shadow for the distances $r_{b1} < r < r_{b2}$. Thus the effectiveness of a barrier with the effect of reflected waves limited by the action of the image barriers can be expressed as

$$IL_{rb} = 10 \log \frac{\overline{p}_0^2 + \sum_{i=1}^{\infty} \overline{p}_{ri}^2}{\overline{p}_d^2 + \sum_{i=1}^{\infty} \overline{p}_{rbi}^2} = IL_d - 10 \log \frac{1 + \left(\sum_{i=1}^{\infty} \overline{p}_{rbi}^2\right)/\overline{p}_d^2}{1 + \left(\sum_{i=1}^{\infty} p_{ri}\right)/\overline{p}_0^2} = IL_d - \Delta IL_b, \tag{31}$$

where ΔIL_b is the decrease of the barrier effectiveness, resulting from the energy of the reflected waves, for the region where the image barriers are effective. Similarly, the effectiveness of a barrier with the effect of the reflected waves limited by the action of absorbing bands becomes

$$IL_{ra} = 10 \log \frac{\overline{p}_0^2 + \sum_{i=1}^{\infty} \overline{p}_{rai}^2}{\overline{p}_a^2 + \sum_{i=1}^{\infty} \overline{p}_{rai}^2} = IL_d - 10 \log \frac{1 + \left(\sum_{i=1}^{\infty} \overline{p}_{rai}^2\right)/\overline{p}_d^2}{1 + \left(\sum_{i=1}^{\infty} \overline{p}_{rai}^2\right)/\overline{p}_0^2} = IL_d - \Delta IL_a, \tag{32}$$

where ΔIL_a is the decrease of the barrier effectiveness due to the presence of reflected waves in the region of the action of the absorbing bands.

In order to examine the above relationships in detail, the following simplifying assumptions will be made:

— The acoustic energy of the waves diffracted at both edges of the absorbing bands and reaching the observer is equal for both paths,

— for reflections of higher order the asymmetrical situation can be replaced by a symmetrical one, by introducing asymmetry coefficients of equation (15): ε_{bi} for the image barriers, and ε_{ai} for the absorbing bands.

In order to account for the affect of reflected waves under the above assumptions, the following coefficients will be introduced:

a coefficient for the waves generated by the i-th image source in conditions without a barrier and without absorbing bands

$$m_i = \frac{\overline{p}_{ri}^2}{\overline{p}_0^2} = \beta^i \cos^2 \gamma_i, \tag{33}$$

where β is the coefficient of reflection of the surface above the barrier before the absorbing band have been placed and γ_i is the angle at which the wave, generated by the i-th image source reaches the observer,

a coefficient representing the influence of the reflected waves at the observation point in the situation when the barrier is installed without absorbing bands

$$\eta_{bs} = \frac{\sum_{i=1}^{\infty} \overline{p}_{rbi}^2}{\overline{p}_0^2} = \sum_{i=1}^{\infty} \frac{m_i}{\varepsilon_{bi}} \frac{\mu}{\mu_{bi}}, \tag{34}$$

a coefficient representing the influence of the reflected waves after the installation of the barrier and the absorbing band for observation points situated in the region where the absorbing band is effective

$$\eta_{as} = \frac{\sum_{i=1}^{\infty} \overline{p}_{rai}^2}{\overline{p}_d^2} = \sum_{i=1}^{\infty} \frac{2\mu}{\mu_{ai}} \frac{m_i}{\varepsilon_{ai}}. \tag{35}$$

Numbers M are related to the Fresnel numbers by relation (6a). M_{bi} and M_{ai} characterize the influence of waves diffracted at the edges of the image barriers and at both edges of the absorbing bands, respectively, whereas M concerns the direct wave diffracted at the edge of the barrier.

Substituting relations (13), (33), and (34) in formula (31), and (13), (33) and (34) — in formula (32), we obtain the following expressions for the decrease of the effectiveness of the barrier due to the reflected waves:

for the region where the image barriers are effective

$$\Delta IL_b = 10 \log \frac{1 + \eta_{bs}}{1 + \sum_{i=1}^{\infty} m_i} = \frac{1 + \sum_{i=1}^{\infty} \frac{\mu m_i}{\mu_{bi} \varepsilon_{bi}}}{1 + \sum_{i=1}^{\infty} m_i}, \tag{36}$$

for the region where absorbing bands are effective

$$\Delta IL_a = 10 \log \frac{1+\eta_{as}}{1+\eta_{as}/M} = 10 \log \frac{1+\sum_{i=1}^{\infty} \frac{2M}{M_{ai}} \frac{m_i}{\varepsilon_{ai}}}{1+\sum_{i=1}^{\infty} \frac{2}{M_{ai}} \frac{m_i}{\varepsilon_{ai}}}, \tag{37}$$

where $M = 20N$ for $N \geqslant 1$ and $M = 20N+3$ for $1 > N > 0$. When the regions, where the image barriers and the absorbing bands are effective, are superposed (Fig. 12b), a double diffraction of the waves generated by the image sources takes place. These conditions correspond to the problem of wave diffraction at two independent barriers which leads to more complicated analytical relationships.

Formulae (36) and (37), despite of the simplifications in their assumption, permit an estimation of the reduction of barrier effectiveness when the propagation of reflected waves is reduced or, inversely, an estimation of the limitation of reflected waves necessary to obtain a required barrier effectiveness.

From a practical point of view this leads to the determination of the width of the absorbing band for given geometrical conditions of the barrier situation and for given conditions of interior.

7. The optimum width of the absorbing band

The choice of the width of the absorbing band depends on the criteria assumed for acoustic conditions behind the barrier. Two different criteria may be used: (a) spatial, (b) energetic (local).

The *spatial criterion* consists in providing an acoustic shadow for the whole area behind the barrier.

It is evident from Fig. 12a that if, due to the joint action of an image barrier and an absorbing band, the whole area behind the barrier will be covered with an acoustic shadow from an image source of the 1st order, this area will be also covered with acoustic shadow from sources of higher orders.

In this case the analysis of the absorbing band action can be limited to the examination of the effect for the first reflection only. For a given room and for assumed barrier parameters it is then most convenient to determine the width of the absorbing band by a graphical method. For the diffraction angle of a wave generated from the image source S', $\psi_a = 0$ (Fig. 13), the rays originating from the image source S' and passing the upper edges of the real and image barriers are drawn. These rays divide the area of action of the barrier and the absorbing band against the reflected waves for any observer point.

The width of the absorbing band d_g is determined by the distance between the above rays. This width will be smallest if the band is mounted on the ceiling.

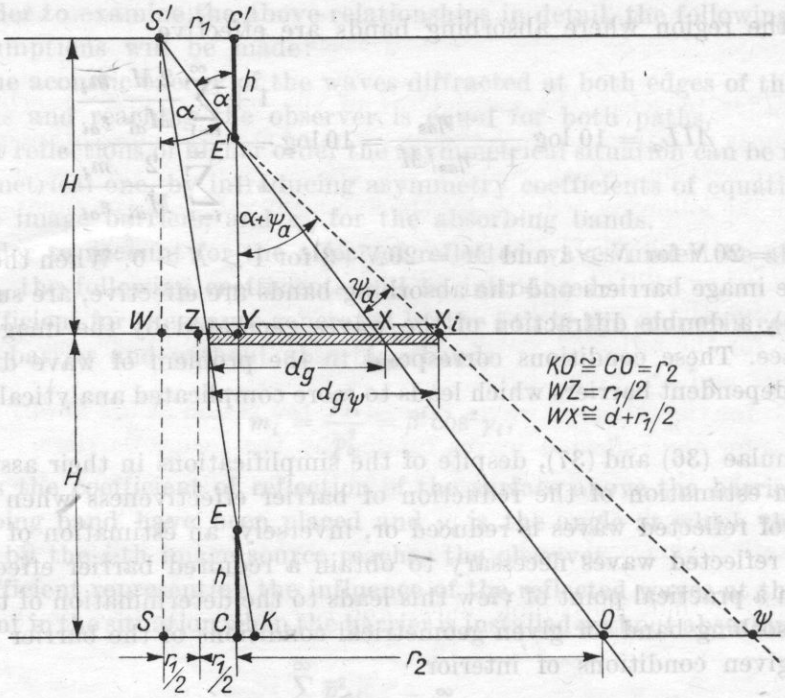

Fig. 13. Illustration of the space criterion for the case of a single reflection

Taking into account the diffraction angle $\psi_a > 0$ (broken line in Fig. 13), the width of the absorbing band should be correspondingly larger. It is evident that when the space criterion is used, the band should be placed asymmetrically above the barrier, and nearer the observer point.

In order to determine analytically the dependence of the width of the band on the system parameters, we make the following simplifications (Fig. 13):

the range of action of the absorbing band

$$KO \cong r_2, \tag{38}$$

the point Z of the absorbing band edge depends only on the distance r_1 between the source and the barrier and is placed half way between them

$$ZY \cong WZ \cong r_1/2, \tag{39}$$

the point X depends on all of the system parameters, namely on the distance r_1 between the source and the barrier, on the barrier height h and on the room height H.

For the angle of diffraction at the image barrier $\psi_a < (90° - \alpha)$ (broken line in Fig. 13) we can write

$$\tan(\alpha + \psi_a) = \frac{d_{g\psi} - r_i/2}{H - h}. \tag{40}$$

Using the formula for the tangent of the sum of two angles, after transformation we obtain

$$d_g = \frac{r_1\left(H-\frac{h}{2}\right)/h+(H-h-r_1^2/2h)\tan\psi_a}{1-r_1\tan\psi_a/h}. \tag{41}$$

For the diffraction angle $\psi_a = 0$ as in Fig. 12a, relation (41) reduces to the following form:

$$d_g = \frac{r_1(H-h/2)}{h}. \tag{42}$$

Usually $H \gg h/2$, and an approximate but simple relation which facilitates practical calculations is obtained:

$$d_g \cong \frac{r_i H}{h}. \tag{43}$$

A comparison of Figs. 14a and 14b shows the Y-shaped barriers to be more effective than the simple ones. For the same effective height of both

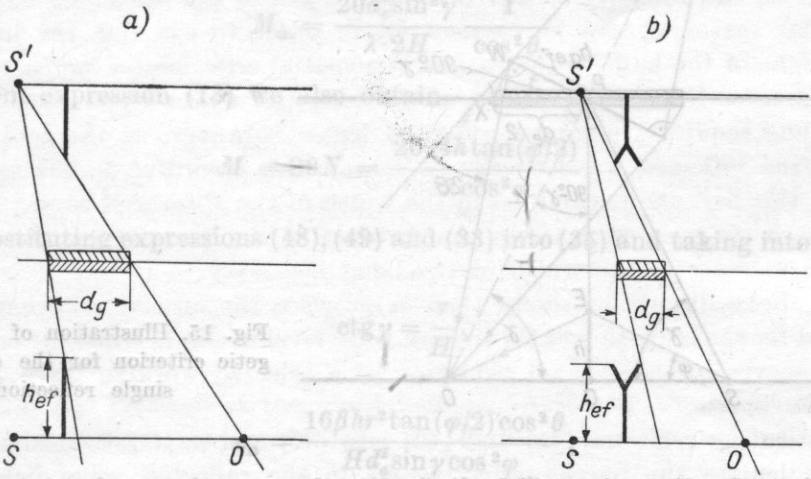

Fig. 14. Comparison of the width of band d_g required for a straight barrier (*a*) and a Y-shaped barrier (*b*) with the same effective height

kinds of barriers the same conditions of acoustic shadow behind the barrier are obtained for a smaller width of absorbing band when a Y-shaped barrier is used.

The *energetic criterion* is based on the ratio of the reflected wave energy to the energy of the diffracted waves, for a chosen observation point. This criterion resolves itself into the choice of a suitable value of the coefficient η_{as} given by formula (35).

Many features of the energetic criterion contrast with those of the spatial criterion. The spatial criterion accounts qualitatively for the joint action of the image barriers and the absorbing bands in order to cover with acoustic shadow as much of the area behind the barrier as possible. This criterion concers points of observation placed rather distantly from the barrier.

In contrast, the energetic criterion is concerned with one chosen point near the barrier and represents quantitatively the action of the absorbing band.

In order to determine the relationship between the required value of the width of the absorbing band for an assumed value of η_a and for the other parameters of the barrier and the room let us make the following simplifying assumptions:

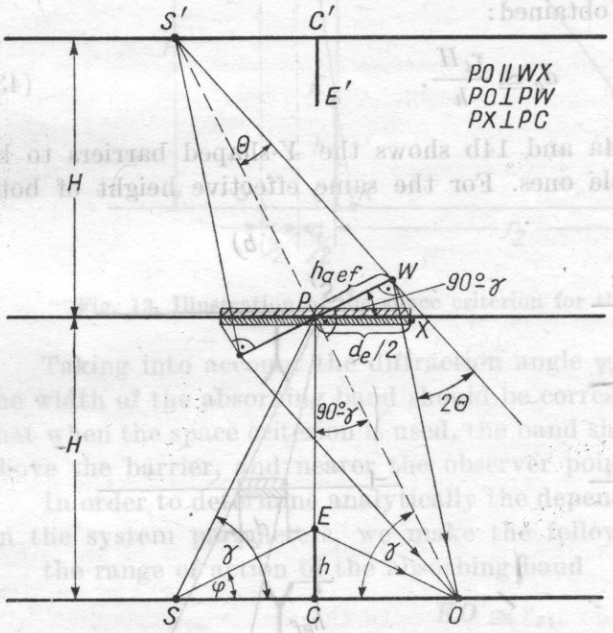

Fig. 15. Illustration of the energetic criterion for the case of a single reflection

at first, the discussion will be limited to the case where only one reflection from the ceiling is taken into account, the floor and other boundaries being absorbing;

the acoustic energy of the waves diffracted at both edges of the absorbing band is the same at the observation point for both paths (Fig. 15);

one half of the width of the absorbing band is replaced by the effective height of the barrier according to the formula

$$h_{aef} = \frac{d_e}{2} \sin\gamma; \tag{44}$$

the angle of diffraction 2θ at the edges of the absorbing band is small; according to the previously accepted criterion of 30° we can assume $\theta \cong 15°$ and then the approximate relation

$$\tan\frac{\theta}{2} \cong \frac{1}{2}\tan\theta; \tag{45}$$

in calculation it will be assumed that (6a) $M = 20N$, $M_a = 20N_a$, which is true only for $N > 1$ and $N_a > 1$. For $N_a < 1$ and $N < 1$ the relations $M_a = 20N_a + 3$ and $M = 20N + 3$ should be used (6b).

Having accepted these simplifications, we may, by (13), write the following relation for M_a:

$$M_a = 20N_a = \frac{20d_e\sin\gamma}{\lambda}\frac{\tan\theta}{\cos^2\theta}. \tag{46}$$

From Fig. 15 we find that

$$\tan\theta = \frac{h_{aef}}{H/\sin\gamma} = \frac{d_e\sin^2\gamma}{2H} \tag{47}$$

and thus

$$M_a = \frac{20d_e^2\sin^3\gamma}{\lambda\cdot 2H}\frac{1}{\cos^2\theta}. \tag{48}$$

From expression (13) we also obtain

$$M = 20N = \frac{20\cdot 4h\tan(\varphi/2)}{\lambda\cos^2\varphi}. \tag{49}$$

Substituting expressions (48), (49) and (33) into (35) and taking into account that

$$\operatorname{ctg}\gamma = \frac{r}{H}, \tag{50}$$

we have

$$\eta_a = \frac{16\beta hr^2\tan(\varphi/2)\cos^2\theta}{Hd_e^2\sin\gamma\cos^2\varphi}, \tag{51}$$

whence

$$d_e = \frac{4r\cos\theta}{\cos\varphi}\sqrt{\frac{h}{H}}\sqrt{\frac{\beta}{\eta_a}}\frac{\tan(\varphi/2)}{\sin\gamma}. \tag{52}$$

Further reduction of formula (52) can be made for the following conditions: $H \gg r$ (thus $\sin\gamma \cong 1$) and $\varphi = \theta < 60°$; then

$$\tan\frac{\varphi}{2} = \frac{1}{2}\tan\varphi \cong \frac{1}{2}\frac{h}{r} \tag{53}$$

and $\cos\theta/\cos\varphi \cong 1$.

Hence we obtain an approximate formula

$$d_e \cong 2h\sqrt{\frac{2r}{H}}\sqrt{\frac{\beta}{\eta_a}}. \tag{54}$$

Assuming $\eta_a = 1$ (which means that $\Delta IL_a = 3$ dB) and $\beta = 1$, we get

$$d_e \cong 2h\sqrt{\frac{2r}{H}}. \tag{55}$$

Comparing this relation with relation (43) for the width d_g we see that their character is contrasting with respect to h and H. This is caused by the previously mentioned differences in the assumptions of the two criteria.

In the case of the spatial criterion a higher barrier provides a greater region of shadow against the reflected wave. Hence, the width of the absorbing band can be smaller.

In the case of the energetic criterion, an increase in the height of the barrier causes a reduction in the effect of the diffracted wave and thereby makes the requirements for the reduction of the effect of the reflected waves more rigorous. This leads to the necessity of increasing the width of the absorbing band.

Similar reasoning can be carried out in order to examine the influence of the height of the hall. In the case of the spatial criterion an increase in hall height increases the area of action of the reflected waves for a given barrier height, thus requiring a larger width of band. However, as the hall height increases the reflected wave energy decreases and, according to the energetic criterion, this permits a reduction in the width of the absorbing band.

In both cases an increase in the distance of the source from the barrier makes an increase in the width of the band necessary.

The above discussion shows that in practice the spatial criterion would be applied for the reduction of the overall noise level in a hall, while the energetic criterion serves for noise level reduction at a selected working place, not far behind the barrier.

Substituting relations (51) and (49) into (37) and next into formula (32), we can calculate the barrier effectiveness in the reflected wave field when the effect of the waves is limited by means of an absorbing band. For a symmetrical situation of the barrier between the source and the observer we obtain

$$IL_{dra} = 10\log\frac{80h\tan\frac{\varphi}{2}}{\cos^2\varphi} - 10\log\frac{1+\dfrac{16\beta hr^2\tan(\varphi/2)\cos^2\theta}{d_e^2 H\sin\gamma\cos^2\varphi}}{1+\dfrac{\lambda\beta r^2\cos^2\theta}{20Hd_e^2\sin\gamma}}. \tag{56}$$

In order to account for multiple reflections between the ceiling and the floor, let us introduce, besides the simplifying assumptions accepted for determin-

ing the coefficients m_i and η_a given for relations (33) and (35), the additional assumptions:

the angle θ_i does not change much for image sources of higher order so that $\cos\theta_i$ does not depend on i;

the effective height corresponding to half of the width of the absorbing band does not depend on the order of the image source.

Then $M_{ai} = M_a = \text{const}$ and (35) becomes

$$\eta_{as} = \frac{2M}{M_a} \sum_{i=1}^{\infty} \frac{m_i}{\varepsilon_{ai}} \ldots \tag{57}$$

From (29) and (57) and the condition $H \gg r$ we obtain

$$\sum_{i=1}^{\infty} \frac{m_i}{\varepsilon_{ai}} \cong (1+\beta)^2 \left(\frac{r}{H}\right)^2 \sum_{i=1}^{\infty} \frac{\beta^{2i-1}}{i^2} \frac{1}{\varepsilon_{ai}}. \tag{58}$$

For higher values of i the ratio $\beta^{2i-1}/i^2 \to 0$. Since.

$$\sum_{i=1}^{\infty} \frac{1}{i^2} \cong \frac{\pi^2}{6} \cong 1{,}64, \tag{59}$$

we can write

$$\eta_{as} < 3{,}28 \frac{M}{M_a} (1+\beta)^2 \left(\frac{r}{H}\right)^2. \tag{60}$$

Taking into account only the first reflection, a value for η_a can be obtained from expression (35) as

$$\eta_a = \frac{2M}{M_a} \left(\frac{r}{H}\right)^2. \tag{61}$$

Thus the increase of the coefficient η_a, caused by the effect of multiple reflections, is equal to

$$s = \frac{\eta_{as}}{\eta_a} < \frac{1{,}64(1+\beta)^2}{\beta}. \tag{62}$$

Putting (62) into formula (37) allows us to evaluate the increase of the effect of the reflected waves due to multiple reflections. From (62) for $\beta = 1$ we obtain $\sqrt{\eta_a} = 0{,}39\sqrt{\eta_{as}}$, which by virtue of (54) gives an increase in the width of the absorbing band of a factor of 2.5. In some cases instead of increasing the width of the band on the ceiling the use of an additional band on the floor may be preferable. Examination of this case is beyond the scope of the present paper, although it was tested experimentally.

When several noise sources are installed in different regions of the room, the screening of each source can be considered individually using the mirror method. When a large number of sound sources is installed in the room the reverberation method is preferable.

8. Experimental results for reflected wave field conditions

Three series of measurements were carried out:

(a) An investigation of the influence of the width of an absorbing band on the effectiveness of the barrier when the ceiling was reflecting.

(b) An investigation of the effectiveness of the absorbing bands when both the ceiling and the floor were reflecting.

(c) An investigation of the effectiveness of the Y-type barrier.

(a) Examination of the effect of the band width of the absorbing band was carried out on a 1 : 8 scale model.

In model the sound absorbing material was mounted on the ceiling. The remaining surfaces were absorbing. The width of the absorbing band was changed from 10 to 140 cm.

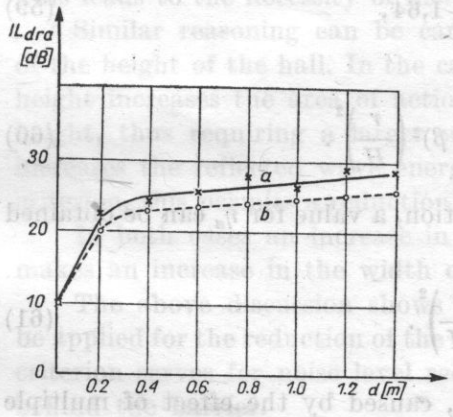

Fig. 16. Barrier effectiveness IL_{dra} versus width of the band

a) experimental results, *b*) calculation results

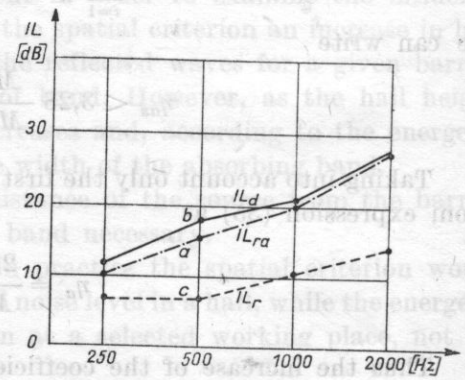

Fig. 17. Experimental results for IL versus frequency:

a) with a reflecting floor and ceiling and an absorbing band on the ceiling (IL_{ra}), *b*) in free field conditions (IL_d), *c*) floor and ceiling reflecting without an absorbing band (IL_{dr})

Measured parameters: height of room $H = 80$ cm, effective height of barrier $h_{ef} = 20$ cm, distance between source or microphone and the barrier in a symmetrical arrangement $r = 20$ cm, reflection coefficient of the ceiling without band $\beta = 1$, coefficient of reflection from absorbing band $\beta_a \cong 0$.

Measurements were performed at a frequency of 8000 Hz which corresponds to 1000 Hz in reality. Fig. 16 presents the analytical results according to (56)

and the measured results. The results show that the measured values of ΔIL_{dra} (curve *a*) are somewhat higher than those calculated (curve *b*).

The value of the width of the absorbing band (calculated from (55)), at which the barrier effectiveness should decrease by 3 dB in relation to anechoic conditions, is equal to

$$d_e = 2 \cdot 20 \sqrt{\frac{2 \cdot 20}{80}} = 28.3 \text{ cm}.$$

For a smaller width, namely for $d_e = 20$ cm, the experimental results show a drop in the ΔIL_{ra} of the barrier by 3 dB relative to anechoic conditions. Thus the measured results are better than the analytical ones.

(b) Measurements were carried out on a 1 : 8 scale model with two reflecting surfaces — the ceiling and the floor — on which absorbing bands were placed.

Measuring parameters: $H = 80$ cm, $r = 20$ cm, $h_{ef} = 20$ cm.

The width of the band d_e calculated from (55) for a single reflection from

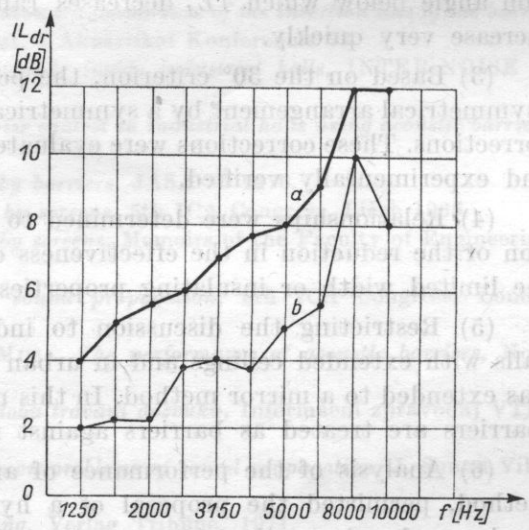

Fig. 18. Experimental results for IL_{dr} of a *Y*-shaped barrier (curve *a*) and a straight barrier (curve *b*) as functions of frequency

ceiling, with a single band, was $d_e = 28{,}3$ cm. The tests were carried out for $d_e = 30$ cm. The experimental results were compared with the results for a free field, with the ceiling and floor totally silenced (curve *b*) as well as with the results when the absorbing bands were removed, i.e. with totally reflecting floor and ceiling surfaces (curve *c*). The results obtained indicate that the performance of the bands is completely satisfactory (Fig. 17).

(c) Comparative measurements of the effectiveness of *Y*-shaped barriers with the same effective height were carried out as initial measurements for further investigations.

Measurements were made in a room with all the walls reflecting. Measuring parameters: room height $H = 2.5$ m, effective height of barrier $h_{ef} = 34$ cm, length of the arms of the Y-barrier $l = 20$ cm. Distance between loudspeaker or microphone and barrier $r = 34$ cm. Fig. 18 illustrates the results obtained. They indicate that the properties of the Y-barrier are better than those of straight barriers and suggest that further investigations in this direction should be made.

9. Conclusions

(1) From the theoretical analysis and data of diagrams in references, which have been confirmed by experimental results, it is necessary to introduce into the formulae for IL_d a correction for the sphericity of the waves. This approximates real conditions but still requires a more detailed study.

(2) Analysis of the curves of IL_d vs. diffraction angle ψ showed that it is helpful to introduce a 30° criterion constituting a limiting value for the diffraction angle below which IL_d decreases rapidly and above which it does not increase very quickly.

(3) Based on the 30° criterion, the possibility was shown of replacing an asymmetrical arrangement by a symmetrical one by the introduction of suitable corrections. These corrections were evaluated, presented in the form of diagrams and experimentally verified.

(4) Relationships were determined to permit the quantitative determination of the reduction in the effectiveness of the barrier in a free field, due to the limited width or insulating properties of the barrier.

(5) Restricting the discussion to individual noise sources in industrial halls with extended ceilings and in urban areas, the method of image sources was extended to a mirror method. In this method the image barriers and band-barriers are treated as barriers against image sources.

(6) Analysis of the performance of an absorbing band, using the mirror method, permitted the proposal of a hypothesis to consider the absorbing band as a barrier against image sources. This hypothesis requires further development but it has permitted the presentation of an analytical method which gives quite good agreement between the analytical and the measured results.

(7) Based on the analytical method developed, relationships for the choice of the width of the absorbing bands were determined according to two different criteria: a spatial criterion and an energetic criterion. From a practical point of view these criteria concern respectively:

— the screening of a wide area behind the barrier ignoring energetic considerations,

— the screening of a certain area of the acoustic field not far behind the

barrier with a given ratio of the energy of the reflected waves to that of waves diffracted by the barrier.

(8) The theoretical discusion was supported by experiments in real and model conditions. The experimental results in general gave values somewhat higher than the analytical ones.

(9) The mirror method developed and used in the paper, despite the introduction of far-reaching simplifying assumptions, permits a good assessment, comparing graphical and analytical methods, of the conditions restricting the reflected waves which reduce the effectiveness of a barrier.

(10) The simplified relationships may be used:

(a) in the desing of industrial interiors to determine conditions suitable for the joint action of barriers together with absorbing bands,

(b) in the design of urban areas by using the criterion of 30°.

References

[1] S. Czarnecki, M. Vogt, E. Glińska, *Comparison of the insertion loss of the barrier walls in free and reverberant field*, Budapest, 5 Akusztikai Konferencia 73.

[2] S. Czarnecki, *Noise control aspects inside industrial halls*, INTER-NOISE 75 Proceedings.

[3] S. Czarnecki, E. Glińska, *Noise control in industrial halls using acoustic barriers*, FASE 75 Proceedings.

[4] U. J. Kurze, *Noise reduction by barriers*, JASA 55 1976.

[5] Z. Maekawa, *Noise reduction by screens*, 5th ICA Congress, Liège 1965.

[6] Z. Maekawa, *Noise reduction by screens*, Memoirs of the Faculty of Engineering, Kobe University No 11 1965

[7] Z. Maekawa, *Environmental sound propagation*, 8th ICA Congress, London 1974.

[8] J. B. Moreland and R. S. Musa, *The performance of acoustic barriers*, Noise Control Engineering **1**, 2 1973.

[9] J. Pujolle, *Novy wzorec pro dobu trávani dozvuku*, Informacni zpravodaj VTEI, VUZORT, **10**, 4 1974.

[10] E. J. Rathe, *Note on two common problems of sound propagation*, J. Sound Vibr., **10**, 3 1969.

[11] W. Schirmer, *Lärmbekämpfung*, Verlag Tribüne, 1971.

[12] S. W. Redfearn, *Some acoustical source-observer problems*, Phil, Mag., ser. 7. 30. 1940.

[13] R. J. Wells, *Industrial acoustics course*. Lecture notes, Acoustic theory II, 253 GL 119-6, 1953.

Received on 15th March 1976

ARCHIVES OF ACOUSTICS
1, 4, 299-308 (1976)

ANALYSIS OF THE INITIAL FRACTION OF BÉKÉSY RECORDINGS IN THE THRESHOLD AUDIOMETRY*

ANTONI JAROSZEWSKI, ANDRZEJ RAKOWSKI

Laboratory of Musical Acoustics, Academy of Music (Warszawa)

Statistical analysis of initial transients in the threshold Békésy tracings, observed mostly at higher rates of the signal level control (i.e. 10 dB/s and 30 dB/s), is given. The transients reach several dB and last about 10 s. Possible background of psychological nature is discussed.

1. Introduction

The new automatic audiometer [8], since its first application more than six years ago in conventional audiometry and psychoacoustical research, has been recognized as a useful tool, having many advantages over commercially available Békésy audiometers [1, 7].

In particular, these are the means used for signal level control, the range of signal control rates, the possibility of increasing the accuracy by using various recording potentiometers to suit the actual demand and, last but not least, integration of the recording and thus its automatic interpolation.

For the proper interpretation of Békésy tracings obtained using the new audiometer, the necessity of gathering statistically significant data pertaining to the normal and (in a limited measure) to pathological hearing was obvious. Among other factors affecting the results in automatic audiometry, the rate of signal level control shows a substantial influence on the tracing. In the new audiometer, the rate of signal level control is changeable over a range much wider than in the commercially available equipment used heretofore, in fact much wider than could be expected to be necessary.

* This work was supported by the Committee of Acoustics of the Polish Academy of Sciences.

The present work is aimed at the normalization of the threshold audiograms for normal hearing at a rate of signal level control 10 dB/s, i.e. 2 to 3 times higher than commonly used in Békésy audiometry in its classic form, and at constant frequencies (disconnected scanning).

2. Apparatus

The audiometer used in the present measurements was set up using standard Brüel and Kjaer equipment [8, 9, 11] and some relatively simple additional units designed in the laboratory. A block diagram of the experimental arrangement is presented in Fig. 1.

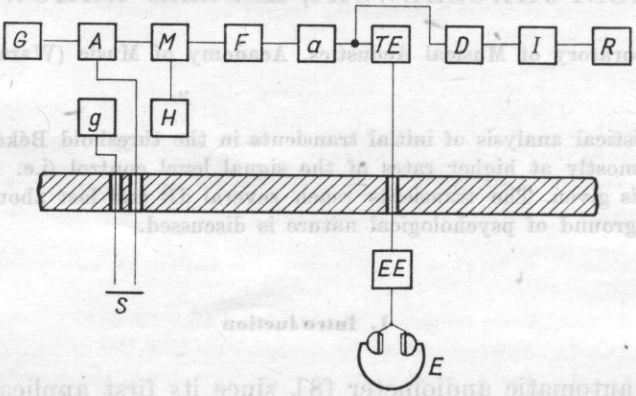

Fig. 1. Block diagram of the audiometric set-up

G – oscillator, *A* – band-pass volume control amplifier, *M* – mixer, *H* – heterodyne, *g* – control signal generator, *S* – control switch, *F* – low-pass filter, *a* – amplifier, *TE* – threshold equaliser, *EE* – earphones equaliser, *D* – detection unit, *I* – integrator, *R* – level recorder, *E* – earphones

The signal level from the oscillator *G* in this system is automatically controlled by the band-pass volume control amplifier *A*. The control signal from a separate external generator *G*, depending on the position of the (push-button) control switch activated by the subject (the listener), varies the amplification factor of the volume control amplifier *A* in such a way that the output signal level varies, i.e. increases or decreases at a predetermined constant rate.

The test signal is obtained from the mixer *M* as a result of mixing signals from the oscillator *G* and from the heterodyne *H*. Although the signal amplitude from the oscillator *G* is controlled by the volume control amplifier *A*, the signal amplitude from the heterodyne *H* is constant.

The signal frequency from the oscillator *G* is 100 kHz and constant, whereas the signal frequency from the heterodyne can be tuned over a range from 100 to 120 kHz, which produces test signals covering the auditory range. The test signal is obviously a frequency difference signal. Signals of the other fre-

quencies resulting from the mixing are filtered out by the low-pass filter *F*. Thus the nonlinear distortions which are usually present in the output of simple volume control amplifier systems are eliminated from the amplitude controlled test signal. Only the isophonic threshold equaliser *TE* and the headphones' frequency response equaliser *EE* for TDH-39 MX-41/AR are used as additional units.

The test signal level, kept near the threshold by the subject by successive reversals of the volume control amplifier action (pushing and releasing the control push-button switch), is automatically recorded by the level recorder *R* operating on the principle of voltage equilibration, after detection and integration in the units *D* and *C*, respectively.

3. Method and subjects

Threshold signal level tracings obtained using the described audiometric system show a transient process in their initial fraction, whose general character may be given by the tracing presented in Fig. 2. Such transients are observed particularly at higher rates of signal level control, i.e. higher than commonly used in the present-day automatic audiometry.

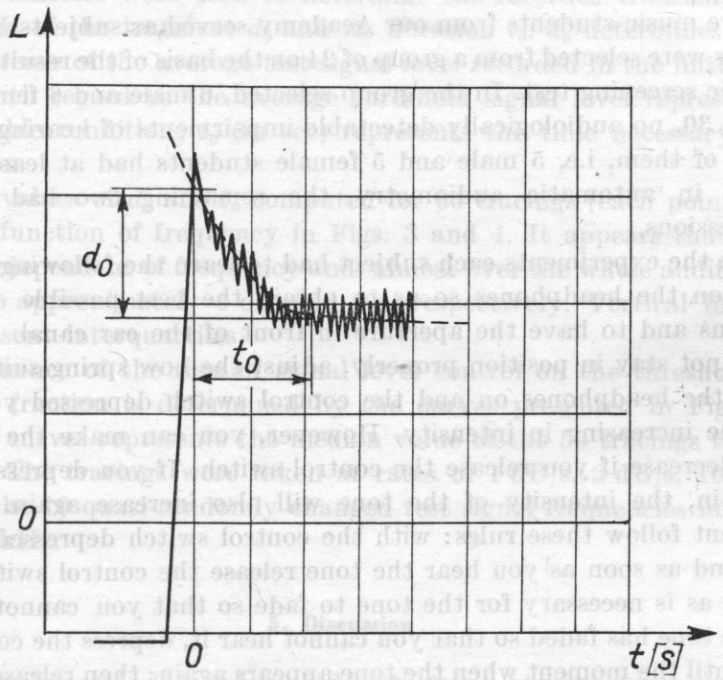

Fig. 2. Initial transient in threshold Békésy tracing
d_0 – amplitude of the transient, t_0 – duration of the transient. Rate of signal level control 10 dB/s

At 1 dB/s the transient is not observed, at 3 dB/s it can be just distinguished in most cases, but at 10 dB/s it is observed quite clearly. The systematic error (constant error) due to the reaction time of the subject at a rate of 10 dB/s should be sufficiently small [6, 10] not to affect the result, and at the same time the operation of the control switch by the subject is not too tiresome even over long periods.

The subjects employed were tested in 30 sessions lasting 1 hr each distributed over a time span of two months. Immediately prior to the measurements each subject was left in a sound isolated booth for 5 min for them to reach the stable threshold after separation from sound sources [2, 3, 4].

In each session up to ten or twenty threshold tracings were usually obtained, each tracing lasting at least 30 s. After each tracing a 5 to 10 min interval was introduced before starting the next one. The duration of the break between the tracings was determined individually by the subject within the specified time limits. The tracings were taken at a constant rate of test signal control, i.e. 10 dB/s, and constant frequencies 40, 80, 160, 300, 500 Hz and 1, 2, 4, 8, 10, 14 kHz.

The frequencies of the test signal were changed from one tracing to the next in a semi-random manner so that the subject did not know which frequency (or pitch) he would hear when starting a new tracing. In that way about 700 tracings were obtained.

Twelve music students from our Academy served as subjects in the experiment. They were selected from a group of 24 on the basis of the results of a routine audiometric screening test. In the group selected, 6 male and 6 female students aged 20 to 30, no audiologically detectable impairments of hearing were observed. Most of them, i.e. 5 male and 5 female students had at least 12 months experience in automatic audiometry, the remaining two had two 1-hour practice sessions.

Before the experiments each subject had to learn the following instruction:

«Put on the headphones so as to obtain the best possible contact with the cushions and to have the aperture in front of the ear canal. If the headphones do not stay in position properly, adjust the bow spring suitably.

With the headphones on and the control switch depressed you will hear a pure tone increasing in intensity. However, you can make the intensity of this tone decrease if you release the control switch. If you depress the control switch again, the intensity of the tone will also increase again. During the measurement follow these rules: with the control switch depressed listen very carefully and as soon as you hear the tone release the control switch but only for so long as is necessary for the tone to fade so that you cannot hear it. As soon as the tone has faded so that you cannot hear it, depress the control switch but only until the moment when the tone appears again; then release the control switch, etc. It is of vital importance for the measurement to keep a rhytmic sequence of increasing and decreasing the intensity of the tone between the

iqmits when you begin to hear the tone and when you are not longer able to hear it. Never allow the tone to become loud and, on the other hand, never allow it to disappear for too long. Release the switch when you just hear the tone and depress it when you just cannot hear it».

To show how much the initial fraction of the threshold tracings is affected by the rate of signal level control, a series of measurements were performed with one very experienced subject. These measurements cover the range of rates of signal level control from 1 dB/s to 30 dB/s. For each rate 50 tracings were taken using the same experimental procedure. The measurements were performed at 10 different frequencies in the range from 40 Hz to 10 kHz. As in the main experiment, the frequencies were set quasi-randomly so that the subject did not know what pitch he would hear after depressing the control switch at the beginning of each tracing.

4. Results

The results of measurements, in the form illustrated in Fig. 2, were further processed according to the commonly used rules, i.e. interpolated (averaged) between the extremes of the recorded spikes. In most cases the curve thus obtained had an exponential character.

Two parameters were used to determine the recorded transients, namely the amplitude of the transient d_0 and its duration t_0. d_0 determines in dB the transient increase of the average test signal level recorded in the initial fraction of tracing with regard to the average threshold signal level representing the following stable condition, t_0 (in sec) represents the time necessary to reach this condition.

Median values of d_0 and t_0 computed for 60 tracings (each point) are presented as a function of frequency in Figs. 3 and 4. It appears that d_0 and t_0 are almost independent of frequency and, almost over the whole auditory range, are equal to approximately 6 dB and 9 s, respectively. Vertical lines in the figures represent interquartiles.

The influence of the rate of signal level control on the threshold tracing in its initial fraction is determined by the curves presented in Fig. 5. Each point on the curves represents the median value of the 50 tracings taken from one subject. The tracings were taken at rates of 1 dB/s, 3 dB/s, 10 dB/s and 30 dB/s for the 10 quasi-randomly changed test signal frequencies in the range 40 Hz to 10 kHz.

5. Discussion

The experimental data presented determine normal transients at the begining of threshold Békésy tracings, with stimulation starting from below the threshold, in the frequency range 40 Hz to 14 kHz and at a rate of signal

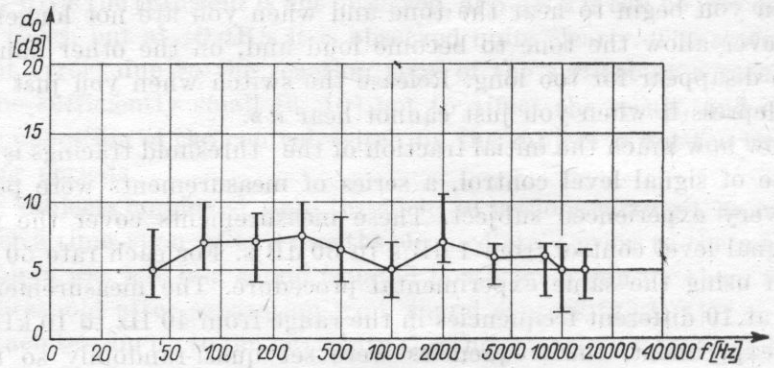

Fig. 3. Initial transient amplitude d_0 in threshold Békésy tracings as a function of frequency at a rate of signal level control 10 dB/s

Frequencies: 40, 80, 160, 300, 500 Hz and 1, 2, 4, 8, 10, 14 kHz. Twelve subjects. Circles are median values and vertical lines interquartiles of 60 tracings each

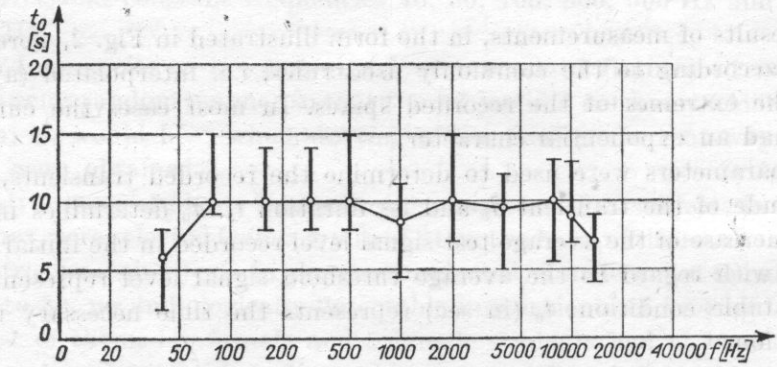

Fig. 4. The duration of the transient t_0 in threshold Békésy tracing at a rate of signal level control 10 dB/s. Subjects, frequencies and symbols as in Fig. 3

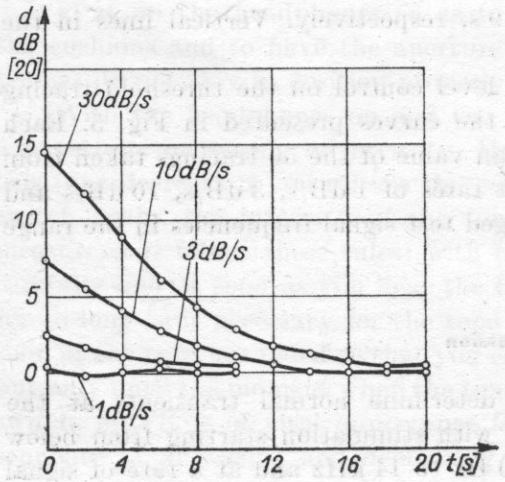

Fig. 5. The dependence of transient amplitude d in threshold Békésy tracings on the rate of signal level control. Circles are medians from 50 tracings from one subject. Frequencies changed semi-randomly in the range 40 Hz - 10 kHz, unknown to the subject; d_0 refers to $t = 0$

level control 10 dB/s. The observed median values of d_0 and t_0 are only a little lower than those obtained earlier from a group of subjects having no experience in automatic audiometry and are practically constant in the frequency range investigated.

These data could lead to the conclusion that, for the detection of a simple tone of unknown frequency, the intensity of this tone must be about 6 dB higher than the intensity at which it could be heard after the detection. In other words, some kind of progressive threshold improvement amounting to about 6 dB seems to take place. However, such an interpretation would be possible only with the assumption that over the whole period of the tracing, the initial fraction included, the tracing produced by the subject represents his «true» threshold, in other words, the tops of the spikes on the tracings always correspond to equally loud sound pulses.

For this reason a control experiment was performed in which pairs of 1 kHz tone pulses with a triangular envelope (analogy to Békésy spikes) of 50 to 100 ms duration and with 250 ms separation were presented to each subject each 3.75 s. The pulses were presented at a level near to the threshold. The subjects had the means to adjust the intensity level of the first pulse in a pair so as to make them equally loud. The results of this experiment showed that equal intensity in the successive pulses corresponded to equal loudness. Thus it seems evident that the transients in Békésy tracings representing intensity changes cannot be assigned to changes of loudness with time.

It seems probable that the mechanism of the process observed could have resulted from a very intense «scanning» of the whole range of the threshold physiological noise, so as to immediately react to the stimulus just as it appeared, but having no information in which region of the frequency scale it can be expected (subjects were not informed which frequency is to be used in the successive tracings). This mechanism, however, differs in its nature from that used after the detection of the stimulus and recognition of its pitch and, subsequently, appearing to the listener in a semi-rhytmic manner which, to some extent at least, could be predicted (regular spikes in the tracing after reaching the stable condition).

In order to get a clearer insight into these mechanisms and, particularly to judge the probability of the «scanning» mechanism suggested, another control experiment was performed with another very experienced subject. This experiment used essentially the same procedure as the main experiment but with two variants, i.e. using semi-randomly varied frequencies unknown to the subject, and using constant frequencies, so that the pitch of test signal to appear was well known to the subject.

Median values of the tracings obtained from the same subject (30 tracings each) for the two variants are presented in Figs. 6 and 7. It can be seen that in the case of a known stimulus, the transient amplitude d_0 is substantially smaller and, at the same time, t_0 shorter. This results probably from the «scan-

ning» being limited to the frequency range proximal to the stimulus frequency, instead of the «scanning» over the whole auditory range. It seems to indicate that the underlying mechanism is rather of a psychological than a physiological nature.

The discrepancies between the data presented in Figs. 5, 6 and 7, particularly with respect to the time scale, result from the fact that in both cases

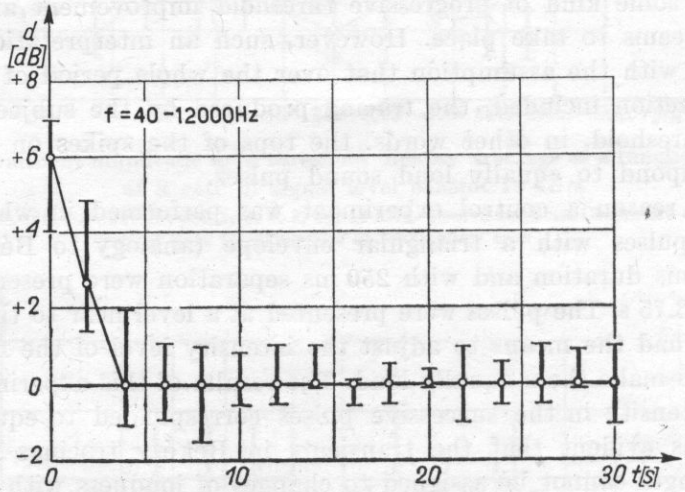

Fig. 6. Transient amplitude d in threshold Békésy tracing. Frequencies changed in the range 40 Hz - 12 kHz. Rate of signal level control 10 dB/s. Data from one subject — 30 tracings. Symbols as in Figs. 3 and 4

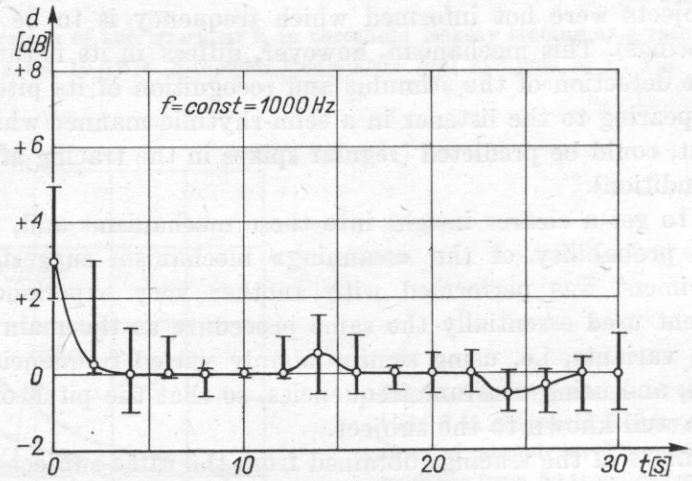

Fig. 7. Transient amplitude d in threshold Békésy tracing at a constant frequency of 1 kHz. Rate of signal level control 10 dB/s. Data from one subject — 30 tracings. Symbols as in Fig. 6

the tracings were taken from one subject only, but that different persons served as subjects in the two experiments.

Still remaining to be discussed is the transient observed even in the tracings at known frequencies. The amplitude of this transient at a rate of signal level control 10 dB/s amounts to about 3 dB. It seems that this transient can be assigned to the reaction times of the subject.

According to SIEGENTHALER [10] the subject's reaction time to pure tone signals at frequencies 250, 1000 and 4000 Hz is of the order of 0.2 s. Thus the transient amplitude of the order of 3 dB at the rate of signal level control 10 dB/s could well have resulted from this factor. It may also be pointed out that Siegenthaler's experiments were carried out at *SL* 40 dB and it is well known that near threshold levels the reaction time is substantially greater.

6. Conclusion

Results of this experiment determine the normal initial transients observed in threshold tracing in automatic audiometry at high rates of test signal level control.

The observed transients seem to result from the specific conditions of the experiment, particularly from the experimental procedure used and high rate of signal control. With regard to the procedure, the presentation of the signals in a semi-random manner over the frequency scale seems to be of importance. The occurrence of these transients can be explained by assuming a «scanning» mechanism in the detection of the test signal embedded in the physiological noise, and the reaction time of the subject (0.2 s), according to SIEGENTHALER. The results presented illustrate well the features of the new audiometer, particularly with respect to the accuracy of the threshold level determination. This is easily achieved by the use of interchangeable recording potentiometers of different ranges and the selection of the suitable rate of signal level control.

References

[1] G. von BÉKÉSY, *A new audiometer*, Acta Otolaryng., **35**, 411 (1947).

[2] M. E. BRYAN, H. D. PARBROOK, W. TEMPEST, *A note on quiet threshold shift in the absence of noise*, J. Sound-Vibration, **2**, 147 (1965).

[3] M. E. BRYAN, H. D. PARBROOK, W. TEMPEST, *Variation of quiet thresholds with low level noise exposure*, Proc. 5th Int. Congress on Acoustics. Liège, **1**, B. 32 (1965).

[4] M. E. BRYAN, W. TEMPEST, *Precision audiometry*, Acta Otolaryngologica, **64**, 205 (1967).

[5] R. FELDTKELLER, E. ZWICKER, *Das Ohr als Nachrichtenempfänger*, S. Hirzel Verl., Stuttgart 1967.

[6] F. HARBERT, I. M. YOUNG, *Amplitude of Békésy tracings with different attenuation rates*, JASA, **39**, 914-919 (1966).

[7] I. S. HIRSH, *Békésy's audiometer*, JASA, **34**, 1333 (1962).

[8] A. RAKOWSKI, A. JAROSZEWSKI, T. ŁĘTOWSKI, *A. Békésy audiometer with standard laboratory equipment* [in Polish], Arch. Akustyki, **4**, 247 (1969).

[9] A. RAKOWSKI, A. JAROSZEWSKI, T. ŁĘTOWSKI, *Automatic audiometer*, Pat. PRL No 138238 [in Polish].

[10] B. M. SIEGENTHALER, *Reaction time, difference limen and amplitude of excursion of normal Békésy audiogram*, J. Auditory Res., **1**, 285 (1961).

[11] A. JAROSZEWSKI, A. RAKOWSKI, *Békésy's audiometer with electronic volume control and its application to the psycho-acoustical measurements* [in Polish], Arch. Akustyki, **11**, 3 (1976).

Received on 25th September 1975

ARCHIVES OF ACOUSTICS
1, 4, 309-322 (1976)

THERMAL EFFECTS IN SOFT TISSUES DEVELOPED UNDER THE INFLUENCE OF FOCUSED ULTRASONIC FIELDS OF SHORT DURATION

LESZEK FILIPCZYŃSKI

Institute of Fundamental Technological Research (Warszawa)

Temperature increases in soft tissues developing under the influence of a concentrated ultrasonic beam, as used in ultrasonography, have been analytically determined. By solving the heat conductivity equation and subsequent use of the Laplace transformation, formulae have been obtained (30), (38) which permit the calculation of the approximate value and distribution of the temperature in the focus of the beam, perpendicular to the direction of propagation, as a function of time.

In the case of an ultrasonic impulse with a duration of 1 μs, the intensity of 20 W/cm², in soft tissue with an attenuation of 3 dB/cm and simplified shape of ultrasonic beam (Fig. 2), a maximum temperature increase equal barely to $3.3 \cdot 10^{-6}$°C has been obtained. The temperature increase calculated for an ultrasonic impulse of 1 s duration gives a value of the same order as that obtained by other authors. In the case of an ultrasonic exposure of an intensity of 200 W/cm² and a duration of 1 s, which corresponds to the threshold from curves for irreversible changes in the brain published in the literature, a value of temperature increase in the tissue of 33°C has been obtained.

1. Introduction

In pulse-echo ultrasonography, used for the visualisation of internal organs of the human body, focused ultrasonic beams are used, the intensity of which, in the focus, may attain a value of 20 W/cm² for the short duration of the impulse about 1 μs.

In investigations concerning the influence of ultrasounds on biological structure this value may reach 1000 W/cm² [5]. No temperature increases are observed in tissues ultrasonically irradiated in this manner, because of the impulse character of radiating fields; the interruption between impulses is about 1 ms and is thus 1000 times as long as the duration of the pulse.

In such a situation the question arises as to whether, in the course of the impulse duration, the tissue region confined by the focus is not temporarily

overheated. This question is important because it is known that even at a temperature of 50°C a permanent damage to the tissues can occur. For instance, we can consider the situation that, in the course of the impulse duration, the temperature has increased by 20°C, but after the longer pause between impulses it has decreased to the original temperature. The high inertia thermometer will, however, in this case indicate only a mean temperature increase three orders of magnitude smaller, and the overheating of the tissues may be not noticed.

We have, therefore, set ourselves the task of estimating the magnitude of the temperature effect arising in the soft tissue under the influence of a focused ultrasonic field of short duration. To simplify the problem we have made some assumptions which will be dealt with in the sequel.

2. Assumptions

Two measurements made of the spatial distribution of the focused ultrasonic field used in ultrasonography of the abdominal cavity at a frequency of 2.5 MHz gave the results shown in Fig. 1. The region of the focus defined by a 3 dB decrease of acoustic pressure relative to the maximum value can, with a good approximation, be described by a cylinder 0.25 cm in diameter and 6.2 cm in length (Fig. 2).

We assume that in the focal region thus defined sources of heat are located with a rate of heat generation per unit volume equal to $\dot{Q}_v$ cal/s·cm³. The size of these sources depends on the intensity of the incident ultrasonic wave as well as on the absorption properties of the tissue. Another simplifying assumption is that of an even distribution of these sources throughout the whole focal region.

In this situation it is convenient to consider the problem in a cylindrical coordinate system. By assuming that the focal region under consideration has a cylindrical shape of infinite lenght the problem is reduced to a two-dimensional one.

In view of the axial symmetry the phenomena considered are solely a function of one coordinate, the radius r. Fig. 3 shows the case considered for the focal region formed in an unlimited biological medium in the shape of an infinite cylinder with the radius R. The temperature of the medium outside the focus is T_o, whereas inside the focus it is T_i. We assume that at the initial moment $t = 0$ the temperatures are equal, i.e. $T_o = T_i = 0$.

3. Initial equations

The absorption of ultrasonic waves will release heat in the focus, thus causing a rise of temperature followed by a flow of heat from the focus into the surrounding biological medium by thermal conduction.

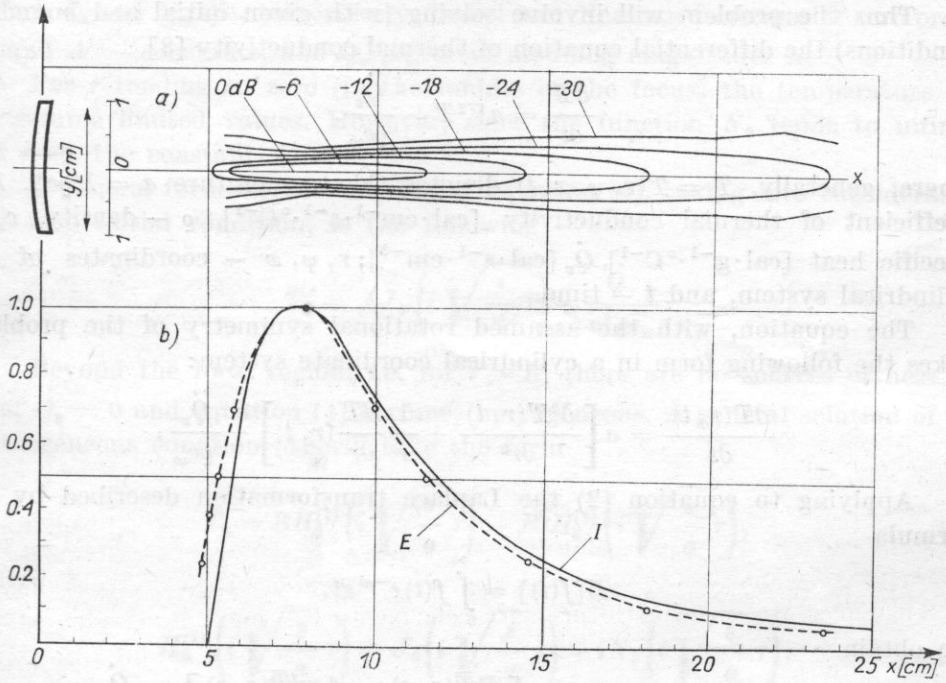

Fig. 1. Measured and calculated distributions of the focused ultrasonic field produced in water by the ultrasonograph UG-4 used for diagnostic examination of the abdominal cavity [2]

a – measured isoecho curves, *b* – computed (*I*) and measured (*E*) intensity distribution along the *x*-axis of ultrasonic beam

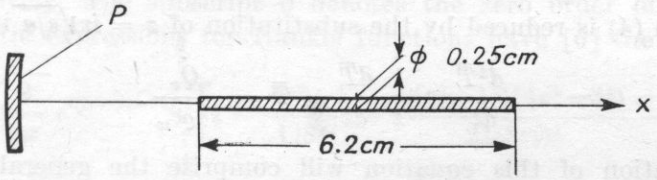

Fig. 2. Approximated shape of the focus region of ultrasonic beam in water described by the 3 dB curve relative to the maximum pressure

x – direction of ultrasonic wave propagation, *P* – transducer radiating the ultrasonic wave

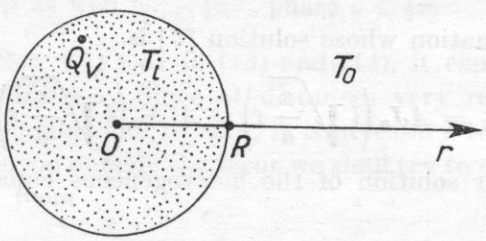

Fig. 3. Dotted focal region with temperature T_i in which heat sources with thermal effect $\dot{Q}_v$ are evenly distributed, and the surrounding region of the medium, $r > R$, with temperature T_0

Thus the problem will involve solving (with given initial and boundary conditions) the differential equation of thermal conductivity [8],

$$\frac{\partial T}{\partial t} = a\nabla^2 T + \frac{\dot{Q}_v}{\varrho c_w}, \tag{1}$$

where, generally, $T = T(r, \psi, x, t)$ denotes the temperature $a = \lambda/\varrho c_w$, λ — coefficient of thermal conductivity [cal·cm^{-1}·s^{-1}·°C^{-1}], ϱ — density, c_w — specific heat [cal·g^{-1}·°C^{-1}], $\dot{Q}_v$ [cal·s^{-1}·cm^{-3}]; r, ψ, x — coordinates of the cylindrical system, and t — time.

The equation, with the assumed rotational symmetry of the problem, takes the following form in a cylindrical coordinate system:

$$\frac{\partial T(r,t)}{\partial t} = a\left[\frac{\partial^2 T(r,t)}{\partial r^2} + \frac{1}{r}\frac{\partial T}{\partial r}(r,t)\right] + \frac{\dot{Q}_v}{\varrho c_w}. \tag{2}$$

Applying to equation (2) the Laplace transformation described by the formula

$$L[f(t)] = \int_0^\infty f(t)e^{-st}dt, \tag{3}$$

we obtain

$$s\overline{T}(r,s) - T(r,t=0) = a\left[\frac{d^2\overline{T}(r,s)}{dr^2} + \frac{1}{r}\frac{d\overline{T}(r,s)}{dr}\right] + \frac{\dot{Q}_v}{s\varrho c_w}, \tag{4}$$

where $\overline{T}$ is the transform $\overline{T}(r,s) = L[T(r,t)]$.

Let us assume that the initial temperature is equal to zero. Then the other component of the left-hand side of equation (4) disappears.

Equation (4) is reduced by the substitution of $z = ir\sqrt{s/a}$ in the equation

$$\frac{d^2\overline{T}}{dz^2} + \frac{1}{z}\frac{d\overline{T}}{dz} + \overline{T} = \frac{\dot{Q}_v}{s^2\varrho c_w}. \tag{5}$$

The solution of this equation will comprise the general homogeneous solution in the form

$$\frac{d^2\overline{T}}{dz^2} + \frac{1}{z}\frac{d\overline{T}}{dz} + \overline{T} = 0, \tag{6}$$

which is a Bessel equation whose solution [6] is

$$\overline{T}_1 = AJ_0\left(i\sqrt{\frac{s}{a}}\,r\right) + A'N_0\left(i\sqrt{\frac{s}{a}}\,r\right); \tag{7}$$

and also a particular solution of the heterogeneous equation whose solution is the expression

$$\overline{T}_2 = \frac{T(r,t=0)}{s} + \frac{\dot{Q}_v}{s^2\varrho c_w}, \tag{8}$$

where J_0 and N_0 are, respectively, Bessel and Neuman functions of zero order, A and A' – constants, and $\dot{Q}_v/\varrho c_w$ is an assumed magnitude.

For r tending to zero (in the middle of the focus) the temperature has to assume limited values. However, since the function N_0 tends to infinity for $r \to 0$, the constant $A' = 0$.

A general form for the solution of equation (4), taking into consideration the zero initial condition, is the following:

$$\overline{T}_i = AJ_0\left(i\sqrt{\frac{s}{a}}\,r\right) + \frac{\dot{Q}_v}{s^2\varrho c_w}. \tag{9}$$

Beyond the focal region, i.e. for $r > R$, there are no sources of heat, so that $\dot{Q}_v = 0$ and equation (4) becomes homogeneous. A general solution of the homogeneous equation (4) will take the form

$$\overline{T}_3 = BH_0^{(1)}\left(i\sqrt{\frac{s}{a}}\,r\right) + B'H_0^{(2)}\left(i\sqrt{\frac{s}{a}}\,r\right), \tag{10}$$

where

$$H_0^{(1)}\left(i\sqrt{\frac{s}{a}}\,r\right) = J_0\left(i\sqrt{\frac{s}{a}}\,r\right) + iN_0\left(i\sqrt{\frac{s}{a}}\,r\right), \tag{11}$$

$$H_0^{(2)} = J_0\left(i\sqrt{\frac{s}{a}}\,r\right) - iN_0\left(i\sqrt{\frac{s}{a}}\,r\right). \tag{12}$$

The functions $H_0^{(1)}$ and $H_0^{(2)}$ are Hankel's functions of the first and second kind, respectively. The subscript 0 denotes the zero order of the function.

Asymptotic expressions for Hankel functions have [6] the form

$$H_v^{(1)}(z) \cong \sqrt{\frac{2}{\pi z}}\, e^{i(z-\pi/4-v\pi/2)}\left[1 - \frac{4v^2-1}{1!8zi} + \frac{(4v^2-1^2)(4v^2-3^2)}{2!(8zi)^2} - \ldots\right], \tag{13}$$

$$H_v^{(2)}(z) \cong \sqrt{\frac{2}{\pi z}}\, e^{-i(z-\pi/4-v\pi/2)}\left[1 + \frac{4v^2-1}{1!8zi} + \frac{(4v^2-1^2)(4v^2-3^2)}{2!(8zi)^2} + \ldots\right] \tag{14}$$

for $|z| \gg 1$, $|z| \gg |v|^2$ as well as $-\frac{1}{2}\pi \leqslant \text{phase } z \leqslant \frac{1}{2}\pi$.

If we substitute $z = i\sqrt{s/a}\,r$ in (13) and (14), it can be seen that $H_0^{(1)} \to 0$ for $r \to \infty$, whereas $H_0^{(2)} \to \infty$. Since at distances very remote from the focus the temperature T should tend to zero, it is necessary to assume that $B' = 0$.

Lastly, in the region outside the focus we shall try to solve the homogeneous equation (4) in the form

$$\overline{T}_0 = BH_0^{(1)}\left(i\sqrt{\frac{s}{a}}\,r\right). \tag{15}$$

The constants A and B which occur in equations (9) and (15) are determined from two boundary conditions which should be satisfied on the boundary surface that divides the considered tissue into the focal region and the outer region.

The first condition of the continuity of the heat flux $\vec{q}$,

$$\vec{q} = -\lambda \operatorname{grad} T, \tag{16}$$

takes the form

$$\frac{d\overline{T}_i}{dr} = \frac{d\overline{T}_0}{dr} \quad \text{for } r = R. \tag{17}$$

Substituting in (17) the expressions for $\overline{T}_i$ from (9) and $\overline{T}_0$ from (15) we obtain

$$\frac{A}{B} = \frac{H_1^{(1)}\left(i\sqrt{\frac{s}{a}}R\right)}{J_1\left(i\sqrt{\frac{s}{a}}R\right)}. \tag{18}$$

In this relation Bessel and Hankel functions of the first order occur as a result of the differentiation of the functions of zero order.

The other condition is the equality of temperatures on each side of the boundary surface, thus

$$\overline{T}_i = \overline{T}_0 \quad \text{for } r = R. \tag{19}$$

Inserting into (19) expressions (9) and (15), we obtain

$$AJ_0\left(i\sqrt{\frac{s}{a}}R\right) + \frac{\dot{Q}_v}{s^2 \varrho c_w} = BH_0^{(1)}\left(i\sqrt{\frac{s}{a}}R\right). \tag{20}$$

From relations (18) and (20) we determine the constant A, namely

$$A = \frac{\dot{Q}_v}{s^2 \varrho c_w} \frac{H_1^{(1)}(i\sqrt{s/a}R)}{J_1(i\sqrt{s/a}R)H_0^{(1)}(i\sqrt{s/a}R) - J_0(i\sqrt{s/a}R)H_1^{(1)}(i\sqrt{s/a}R)}. \tag{21}$$

Now we can finally calculate the transform of the required temperature $\overline{T}_i$ of the focus from relations (9) and (21) and obtain

$$\overline{T}_i = \frac{\dot{Q}_v}{s^2 \varrho c_w}\left[1 + \frac{\pi}{2}\sqrt{\frac{s}{a}}RH_1^{(1)}\left(i\sqrt{\frac{s}{a}}R\right)J_0\left(i\sqrt{\frac{s}{a}}r\right)\right]. \tag{22}$$

4. The temperature in the focal region of the ultrasonic field

The inverse transform of expression (22) can be determined by virtue of the theorem of the homology between the transformed function and its transform [8]:

$$L[f(at)] = \frac{1}{a}\bar{f}\left(\frac{s}{a}\right). \tag{23}$$

From the foregoing it can be concluded that high values of the argument $i\sqrt{s/a}R$ will correspond to small values of at/R^2. Small values of at/R^2 are the subject of our interest since the heat conductivity of soft tissues is insignificant. Furthermore, we are interested in ultrasonic impulse of short duration.

Therefore, when evaluating the inverse transform, we expand expression (22) into a series by taking advantage of the asymptotic expressions (13) and (14) for Hankel functions of large arguments, and the following expressions [8] for Bessel functions:

$$J_0(iz) \cong \frac{e^z}{\sqrt{2\pi z}}\left(1 + \frac{1^2}{1!(8z)} + \frac{1^2\cdot 3^2}{2!(8z)^2} + \frac{1^2\cdot 3^2\cdot 5^2}{3!(8z)^3} + \ldots\right), \tag{24}$$

$$J_1(iz) \cong \frac{ie^z}{\sqrt{2\pi a}}\left(1 - \frac{1\cdot 3}{1!8z} - \frac{1\cdot 3\cdot 5}{2!(8z)^2} - \frac{1^2\cdot 3^2\cdot 5\cdot 7}{3!(8z)^3} - \ldots\right). \tag{25}$$

Substituting (13), (14), (24) and (25) into (22) we obtain

$$\bar{T}_i = \frac{Q_v}{s^2\varrho c_w}\left\{1 - \frac{\exp[-\sqrt{s/a}\,(R-r)]}{2}\sqrt{\frac{R}{r}}\left[1 + \frac{1}{\sqrt{s/a}}\left(\frac{1}{8R} + \frac{3}{8R}\right) + \right.\right.$$

$$\left.\left. + \frac{1}{s/a}\left(\frac{9}{128r^2} + \frac{3}{64Rr} - \frac{15}{128R^2}\right) + \ldots\right]\right\}. \tag{26}$$

Having taken advantage of the relations (see [8])

$$L^{-1}\left[\frac{\exp[-\sqrt{s/a}\,x]}{s^2}\right] = 4t\,\mathrm{int}^2\mathrm{erfc}\,\frac{x}{2\sqrt{at}}, \tag{27}$$

$$L^{-1}\left[\frac{[\exp[-\sqrt{s/a}\,x]}{s^2\sqrt{\dfrac{s}{a}}}\right] = 8t\sqrt{at}\,\mathrm{int}^3\mathrm{erfc}\,\frac{x}{2\sqrt{at}}, \tag{28}$$

$$L^{-1}\left[\frac{\exp\left[-\sqrt{\dfrac{s}{a}}\,x\right]}{s^3}\right] = 16t^2\,\mathrm{int}^4\mathrm{erfc}\,\frac{x}{2\sqrt{at}}, \tag{29}$$

where

$$\operatorname{erfc} a = 1 - \operatorname{erf} a = \frac{2}{\sqrt{\pi}} \int_a^\infty e^{-u^2} du \tag{29a}$$

as well as

$$\operatorname{int}\operatorname{erfc} a = \int_a^\infty \operatorname{erfc} u du, \tag{29b}$$

we can calculate the inverse transformation of expression (26). As result we obtain an expression for the temperature T_i at focal region ($r \leqslant R$):

$$T_i = \frac{\dot{Q}_v t}{\varrho c_w}\left\{1 - \frac{1}{2}\sqrt{\frac{R}{r}}\left[4\operatorname{int}^2\operatorname{erfc}\frac{(R-r)}{2\sqrt{at}} + \sqrt{at}\operatorname{int}^3\operatorname{erfc}\frac{(R-r)}{2\sqrt{at}} \times \left(\frac{1}{r} + \frac{3}{R}\right) + \right.\right.$$
$$\left.\left. + \left(at\operatorname{int}^4\operatorname{erfc}\frac{(R-r)}{2\sqrt{at}}\right)\left(\frac{9}{8r^2} + \frac{3}{4Rr} - \frac{15}{8R^2}\right) + \ldots\right]\right\}. \tag{30}$$

This formula is not valid for very small values of r, since in this case the expansion (24) is not valid.

When the heat conductivity of a biological medium tends to zero ($a \to 0$), and the boundary surface ($r \neq R$) is neglected, square bracket of expression (29) disappears, since then we have $\operatorname{erfc}\infty = 0$ whence likewise

$$\operatorname{int}^n\operatorname{erfc}\infty = 0. \tag{31}$$

A similar result is obtained from expression (30) at a finite value of heat conductivity ($a \neq 0$), when the time tends to zero. In this case the temperature of the medium is

$$T_i = \frac{\dot{Q}_v t}{\varrho c_w} \quad (a = 0) \tag{32}$$

and

$$\frac{dT_i}{dt} = \frac{\dot{Q}_v}{\varrho c_w} \quad (a \neq 0, t = 0). \tag{33}$$

When we substitute the magnitude of $\dot{Q}_v$ from (37) into (33), we get the expression quoted by FREY [4].

On the boundary surface of the focus ($r = R$) we obtain from formula (30) a value of temperature equal to

$$T_i = \frac{\dot{Q}_v}{\varrho c_w} t\left[\frac{1}{2} - \frac{1}{3R}\sqrt{\frac{at}{\pi}}\right]. \tag{34}$$

In view of the fact that water accounts for 75 % of soft tissue content, we may approximate by assuming such parameters for soft tissue as are encoun-

tered in water. Thus, we have at a temperature of 30°C the value of the heat conductivity factor equal to $\lambda = 0.00038$ cal/cm.s °C [7]. In this case the value of the coefficient a is

$$a = \frac{\lambda}{\varrho c_w} = 0.00038 \text{ cm}^2/\text{s}. \tag{35}$$

Fig. 4 shows the temperature distribution in the region of the focus, as evaluated from formula (30), as a function of radius $r (r \leqslant R = 1.25$ mm) for various durations of the impulse t and also with the assumption of a zero value of the coefficient a, using expression (32).

To determine the value of the temperature T_i in the case of impulse ultrasonography considered by us, we calculate the rate of heat generation per unit volume $\dot{Q}_v$ in the focal region. Let us consider an infinitesimal focal region in the form of a cylinder of length Δx (Fig. 5). The intensity of a plane ultrasonic wave I_x [W/cm²] propagating along the x-axis decreases exponentially according to the relation

$$I_{x+\Delta x} = I_x e^{-2a\Delta x}, \tag{36}$$

where a denotes the pressure coefficient of the attenuation of ultrasound. The quantity $\dot{Q}_v$ is defined as the ratio of the amount of heat released per unit time to the volume of the region $A\Delta x$

$$\dot{Q}_v = k \frac{E_x - E_{x+\Delta x}}{\Delta t \cdot A \Delta x} = k \frac{I_x - I_{x+\Delta x}}{\Delta x}, \tag{37}$$

where A denotes the cross-section of the focus, E_x – the energy of the progressive wave, and $k = 0.24$ cal/W$_s$.

Substituting (36) into (37) we finally obtain

$$\dot{Q}_v = kI_x \frac{(1 - e^{-2a\Delta x})}{\Delta x} = 2kaI_x \quad \text{for } \Delta x \to 0. \tag{38}$$

From this it can be seen that the thermal effect of the heat source is dependent on I_x. We will thus consider the end of the focal region closest to the transducer shown in Fig. 2, where the value of the intensity of ultrasound is assumed to be equal to 20 W/cm². Assuming an attenuation coefficient in soft tissues of 3 dB/cm, we have $a = (3 \text{ dB/cm})(8.67 \text{ dB})^{-1} = 0.34 \text{ cm}^{-1}$. Hence we obtain the maximum value $\dot{Q}_v = 14k$ W/cm³, and also $\dot{Q}_v/\varrho c_w = 3.3$°C/s.

For ultrasonic impulses of duration 1 μs we obtain, from formula (32), a maximum temperature increase in the focus barely equal to $T_i = 3.3 \cdot 10^{-6}$ °C.

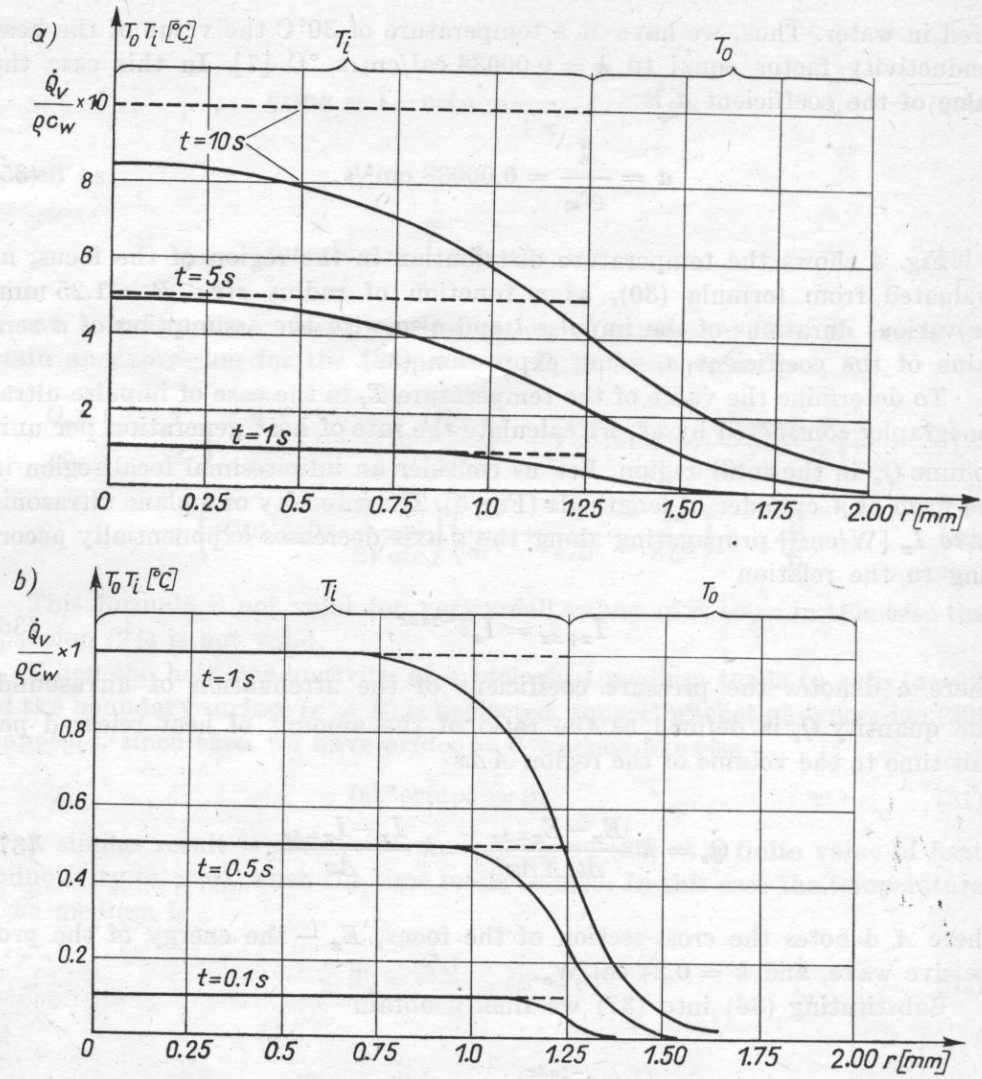

Fig. 4. The temperature distribution in the focal region $r < 1.25$ mm and beyond the focus $r > 1.25$ mm computed from formulae (30) and (41) as a function of the radius r at various durations t of ultrasonic irradiation for $a = 0.00038$ cm^2/s (continuous curve) and for $a = 0$ (broken curves)

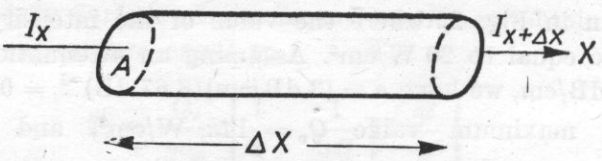

Fig. 5. The intensity of the wave passing through an element the focal region, with length Δx and cross-sectional area A

5. The temperature beyond the region of the ultrasonic focus

This temperature is determined on the basis of formula (15) by evaluating the constant B from expressions (18) and (30). Then we have

$$\overline{T}_0 = \frac{\dot{Q}_v}{s^2 \varrho c_w} \frac{\pi}{2} \sqrt{\frac{s}{a}}\, R J_1\left(i\sqrt{\frac{s}{a}}\, R\right) H_0^{(1)}\left(i\sqrt{\frac{s}{a}}\, r\right). \tag{39}$$

The inverse transform of this expression is determined in a similar manner as before by using series expansions (13), (14), (24), (25) of Bessel and Hankel functions and relations (27)-(29). Then we have

$$\overline{T}_0 = \frac{\dot{Q}_v}{s^2 \varrho c_w} \frac{1}{2} \sqrt{\frac{R}{r}} \exp\left[-\sqrt{\frac{s}{a}}\,(r-R)\right]\left[1 - \frac{1}{\sqrt{\frac{s}{a}}}\left(\frac{1}{8r} + \frac{3}{8R}\right) + \right.$$

$$\left. + \frac{1}{\frac{s}{a}}\left(\frac{9}{128r^2} + \frac{3}{64rR} - \frac{15}{128R^2}\right) - \ldots\right], \tag{40}$$

whence we obtain the final temperature beyond the region of the focus ($r \geqslant R$) equal to

$$T_0 = \frac{\dot{Q}_v t}{\varrho c_w} \frac{1}{2} \sqrt{\frac{R}{r}}\left[4\,\mathrm{int}^2\mathrm{erfc}\frac{r-R}{2\sqrt{at}} - \left(\frac{1}{r} + \frac{3}{R}\right)\sqrt{at}\,\mathrm{int}^3\mathrm{erfc}\frac{r-R}{2\sqrt{at}} + \right.$$

$$\left. + \left(\frac{9}{r^2} + \frac{6}{rR} - \frac{15}{R^2}\right)\frac{at}{8}\,\mathrm{int}^4\mathrm{erfc}\frac{r-R}{2\sqrt{at}} - \ldots\right]. \tag{41}$$

It can be easily seen that on the boundary surface of the focal region ($r = R$) we obtain from formula (41), as expected, the same value as expressed already by formula (34).

Fig. 4 also shows the temperature distribution calculated beyond the focal region ($r \geqslant R = 1.25$ mm) as a function of the radius r for various durations t of the ultrasonic impulse.

6. Conclusions

In the range of impulse ultrasonography, in which the impulse duration is about 1 μs, the temperature increase of the medium during the pulse duration is of the order of 10^{-6}°C. For an intensity $I = 20$ W/cm² the temperature calculated by us was barely $3.3 \cdot 10^{-6}$°C. This increase is entirely negligible.

At the intensities assumed and times of ultrasonic radiation equal to 1 s the temperature increases can attain a value of 3.3°C, thus at the times of this order they may cause irreversible changes in the tissues irradiated by the ultrasound.

The temperature increase in the middle of the focus does not depend on the thermal conductivity for short duration of ultrasonication (in our case for $t < 5$ s, Fig. 4a). The thermal conductivity then influences only the temperature distribution in the proximity of the focal boundary.

The temperature distribution in the focus shown in Fig. 4 is an approximated distribution by virtue of the assumed stability of the intensity of ultrasound in the focus for $0 \leqslant r \leqslant R$. In reality, because of decreasing intensity in the focus along the coordinate r, the temperature will decrease for considerably smaller values of r and this decrease will occur more evenly. The distribution can also be modified by heat flow along the x-axis of the focus and this has not been considered in this paper.

In the case of tissues well supplied with blood one should consider the additional factor of heat transfer by the blood causing a temperature decrease of the tissues. This problem was also not considered in this paper.

A number of simplifications assumed in the paper, chiefly in the range of the field distribution, is not of any great importance in view of the purpose of the paper, namely the evaluation of the thermal effect encountered in tissues.

The estimates obtained are approximately in agreement with the experimental results obtained in the tissues of mammalian muscles by FREY [3], where, with the aid of thermocouple probes, a temperature increase of 2.9°C has been measured at an intensity of 64 W/cm² for 1 s.

It is also of interest to compare the results obtained with the threshold curves for ultrasonic doses causing irreversible structural changes in mammalian brain [1]. From the curves presented in the cited paper, there is, at a frequency of 3 MHz, a threshold value at an intensity of 200 W/cm² with ultrasonic impulses of duration 1 s. On the basis of formulae (32) and (38) we would then obtain a temperature increase in the focus of 33°C, a temperature that would doubtless cause damage to the tissues.

References

[1] F. DUNN, J. E. LOBNES, F. J. FRY, *Frequency dependence of threshold ultrasonic dosages for irreversible structural changes in mammalian brain*, JASA, **58**, 2, 512-514 (1975).

[2] L. FILIPCZYŃSKI, G. ŁYPACEWICZ, J. SAŁKOWSKI, *Intensity determination of focused ultrasonic beams by means of electrodynamic and capacitance methods*, Proc. Vibration Problems, **15**, 4, 297-305 (1974).

[3] W. J. FRY, R. B. FRY, *Temperature changes produced in tissue during ultrasonic radiation*, JASA, **25**, 6-11 (1953).

[4] W. J. FRY, R. B. FRY, *Determination of absolute sound levels and acoustic absorption coefficients by thermocouple probes. Theory*, JASA, **26**, 3, 294-310 (1954).

[5] R. C. Hill, G. P. Joshi, S. H. Revell, *A search for chromosome damage following exposure of Chinese hamster cells to high intensity pulsed ultrasound*, British Journ. of Radiology, 45, 333 (1972).

[6] N. W. McLachlan, *Bessel functions for engineers* [in Polish], PWN, Warszawa 64.

[7] *Physico-chemical handbook* [in Polish], WNT, Warszawa 1974.

[8] H. Tautz, *Wärmeleitung und Temperaturausgleich*, Akademie-Verlag, Berlin 1971.

Received on 28th November 1975

ARCHIVES OF ACOUSTICS
1, 4, 323-335 (1976)

THE RELATION OF THE SPECIFIC ACOUSTIC IMPEDANCE OF LIQUIDS AND THE SURFACE TENSION

BOGDAN NIEMCZEWSKI

Tele- and Radio Research Institute (Warszawa)

Theorems for the dependence of the specific acoustic impedance (ϱc) of organic liquids on the surface tension (σ) are proposed and substantiated. It was found that for a given liquid the quotient $N = \varrho c/\sigma$ is constant at different temperatures. For liquids with similar chemical structure $N = \varrho c/\delta \approx$ const.

Formulae for the sound propagation velocity and its temperature coefficient which permit the evaluation of the said parameters from the density and surface tension of a liquid are given. An analysis of the accuracy of the values of sound velocities has been made and the temperature coefficients $\Delta c/\Delta t$, calculated for ten liquids, have been compared with the coefficients obtained by experiment. A reversal of the relationship for N permits calculation of the surface tension with an accuracy that is sufficient for practical purposes.

It has long been known that there exists an intimate relationship between the sound velocity in a liquid and the surface tension of this liquid, and attempts have been made to express this relationship in a mathematical form. K. ALTENBURG has calculated the velocity of elastic waves in a liquid to be equal to

$$c = 5.663\sqrt{\sigma}\sqrt[6]{\frac{6.024\cdot 10^{23}}{\varrho_l^2 M}}\,\frac{\varrho_l}{\varrho_l - \varrho_g},$$

where σ denotes the surface tension in dynes/cm, ϱ_l — the liquid density in g/cm^3, ϱ_g — the density of gas adjoining the liquid in g/cm^3, and M — the molecular weight of the liquid.

Calculations made using this formula are, however, arduous, and the results are not always confirmed by experiment.

On the other hand, there is no information in the literature on attempts to relate the surface tension with the acoustic impedance although the establishment of such a dependence seems obvious. This problem, particularly for organic liquids, has been the subject of the investigations which are reported in the sequel.

On the basis of calculations made for over one hundred organic liquids (the initial data and the results for some of these liquids are given in the subsequent tables) we have come to the following conclusions:

1. The quotient of the specifics acoustic impedance (ϱc) and the surface tension (σ) for a given organic liquid have a constant value which is independent of temperature, i.e. $\varrho c/\sigma = \text{const}$.

2. The quotient of the specific acoustic impedance and the surface tension for organic liquids of similar chemical structure, which do not contain in their molecules atoms other than C, H, O and N, are approximately constant, i.e. $\varrho c/\sigma \approx \text{const}$.

3. The quotient of the specific acoustic impedance and the surface tension for organic liquids, which contain in their molecules, in addition to atoms of C and, eventually, H, O and N, other atoms but of the same element for all of these liquids, are functions of the weight content of this element in the molecule, i.e.

$$\frac{\varrho c}{\sigma} = f\left(\frac{nm}{M}\right),$$

where n denotes the number of atoms of the element other than C, H, O and N in the molecule, m the atomic weight of this element, and M the molecular weight of the liquid.

Denoting by the letter N the value of the expression $\varrho c/\sigma$, in which we will substitute values of c in m/s (for the sake of simplicity), ϱ in g/cm^3 and σ in dynes/cm, we obtain:

$N \approx 38.5$ for unbranched chain hydrocarbons (Table 1),
$N \approx 39.6$ for ketones,
$N \approx 40.0$ for cyclic substances and branched chain hydrocarbons (Tab l 2),
$N \approx 40.7$ for unbranched alcohols,
$N \approx 42.7$ for branched alcohols,
$N \approx 42.9$ for unbranched carboxylic acids,
$N \approx 43.7$ for esters (Table 3).

The presence of trivalent nitrogen or unsaturated bonds in a chain or ring in a liquid molecule in most cases reduces the numerical value N, while the presence of more than two atoms of oxygen in the molecule increases it.

The value of N for organic liquids, that contain in their molecules atoms of elements other than C, H, O and N, increases exponentially with the weight content of this element in the molecule. This is shown in Tables 4 and 5 and in Fig. 1. The constancy of the numerical value of N with changing temperature has been proved in a sample of twelve organic liquids in Fig. 2. Small and insignificant differences are probably caused by insufficient accuracy of values of parameters taken from the tables.

The values of the parameter N at various temperatures for water have also been calculated. The results are shown in Fig. 2. It was found that within

a range from 0 to 100°C the value of N for water increases from 18.55 to 25.13.

Liquid gases H_2, O_2 and N_2 exhibit a similar dependence of N on the temperature. Lack of sufficient data does not permit the investigation of this problem in as many cases as would be needed to draw universal conclusions about the function $N = f(t)$ for inorganic liquids. However, it does not seem that all of them should behave in a similar manner to water and the liquid gases. For example, Table 6 gives the results of a calculation made for mercury. Within the temperature range from 0 to 200°C, the value of N for mercury is perfectly constant (the deviation from the mean does not exceed 0.08 %). At temperatures no lower than about 250°C N shows a gradual which rise in the proximity of the boiling point (357°C) reaches about 5 %. However, it is not clear if there is a real deviation of the value of N from a constant value or whether the values of sound velocity used for the calculation were already overstated. They were calculated on the basis of the coefficient $\Delta c/\Delta t = 0.464$ m/s·deg, cited after HUBBARD and LOOMIS by SCHAAFFS, and measured in the temperature range from 0 to 70°C. The extrapolation for the value of c above 200°C is thus risky.

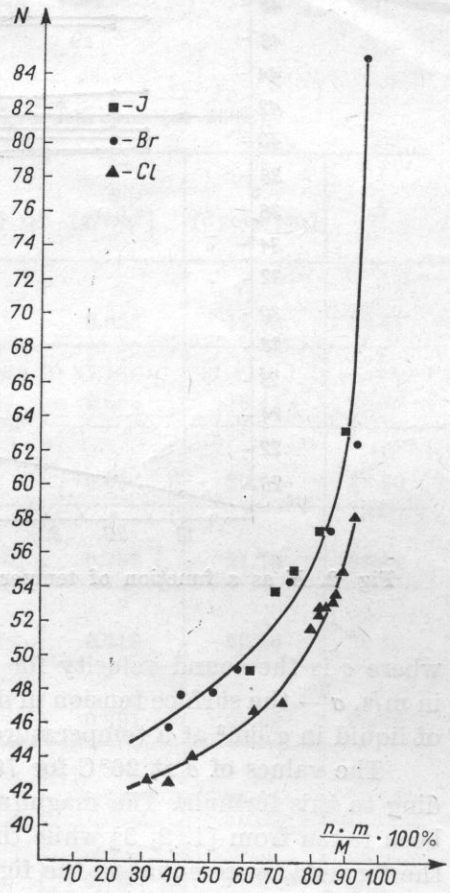

Fig. 1. N as a function of the percentage content of Br, Cl and J in molecules of organic liquids

The rules presented in this paper provide a simple method to evaluate any of the parameters involved in the formula $\varrho c = N\sigma$ from the other parameters, if they are known for a given temperature. Furthermore, this relation can be useful in investigating the properties of various organic liquids, and also permits a new look at the essence of the acoustic impedance of a liquid.

On the basis of the relations presented we may write, at a temperature t°C, the equality

$$c = \frac{N\sigma}{\varrho}, \tag{1}$$

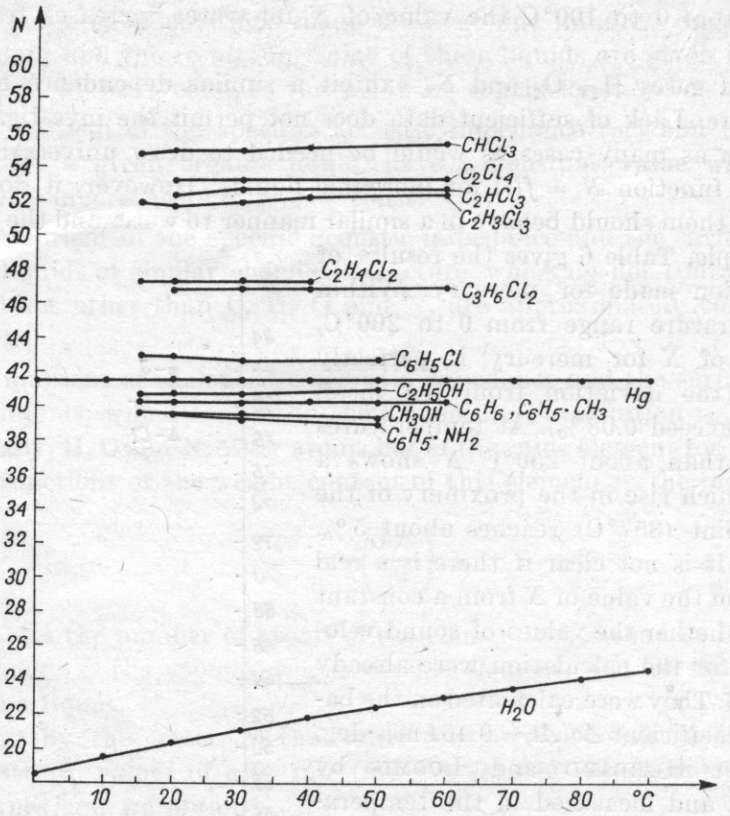

Fig. 2. N as a function of temperature for 12 organic liquids, mercury and water

where c is the sound velocity for a given organic liquid at a temperature t°C in m/s, σ — the surface tension in dynes/cm at temperature t°C, ϱ — the density of liquid in g/cm³ at a temperature t°C.

The values of c at 20°C for 70 organic liquids have been calculated according to this formula. The magnitudes of the surface tension and density have been taken from [1, 2, 3] while the values of the parameter N, substituted in the formula, were equal to the figures given above. The results obtained have been compared with sound velocities as stated in a standard reference book [4]. The differences between the calculated and measured values of c as follows:

Difference m/s	0-10	11-20	21-30	31-40	41-50	over 50
Number of liquids	36	17	9	5	2	1
%	51.4	24.3	12.9	7.1	2.9	1.4

The mean difference of the calculated and measured sound velocities for seventy organic liquids is 15 m/s and this corresponds to 1-2 % of the mean sound velocity of these liquids.

The formula for the temperature coefficient $\Delta c/\Delta t$ of the sound velocity can be derived by simple transformations of formula (1) for the sound velocity.

For temperatures t_1 and t_2:

$$c_1 = \frac{N\sigma_1}{\varrho_1} \quad \text{and} \quad c_2 = \frac{N\sigma_2}{\varrho_2}.$$

Table 1. N for unbranched paraffin hydrocarbons (at 20° C)

Hydrocarbon	c [m/s]	ϱ [g/cm^3]	σ [dynes/cm]	N
C_5H_{12} n-pentane	1030	0.626	16.63	38.77
C_6H_{14} n-hexane	1083	0.659	18.41	38.77
C_7H_{16} n-heptane	1154	0.684	20.29	38.90
C_8H_{18} n-octane	1192	0.702	21.78	38.42
C_9H_{20} n-nonane	1234	0.718	22.96	38.59
$C_{10}H_{22}$ n-decane	1255	0.731	23.89	38.40
$C_{12}H_{26}$ n-dodecane	1300	0.750	25.48	38.26
$C_{14}H_{30}$ n-tetradecane	1331	0.763	26.66	38.09
$C_{16}H_{34}$ n-hexadecane	1363	0.776	27.64	38.27

Mean N: 38.50 ± 0.4 ($0.4 \approx 1.0\,\%$)

Subtracting both sides of these formulae we obtain

$$c_1 - c_2 = N\left(\frac{\sigma_1}{\varrho_1} - \frac{\sigma_2}{\varrho_2}\right).$$

Table 2. N of branched hydrocarbons and cyclic substances (at 20°C)

Substance	c [m/s]	ϱ [g/cm^3]	σ [dynes/cm]	N
1	2	3	4	5
C_6H_{10} cyclohexane	1305	0.811	26.55	39.9
C_6H_{12} cyclohexane	1277	0.779	24.95	39.9
C_6H_6 benzene	1324	0.879	28.87	40.3
C_7H_8 toluene	1328	0.867	28.53	40.4
C_8H_{10} m-xylene	1343	0.864	28.9	40.1
C_8H_{10} p-xylene	1334	0.861	28.37	40.5
C_8H_{10} o-xylene	1364	0.880	30.03	40.0
C_8H_{10} ethylobenzene	1338	0.868	29.2	39.8
C_9H_{12} proplylobenzene	1342	0.878	29.10	40.5
C_9H_{12} 1,2,3-trimethylobenzene	1372	0.894	31.27	39.2
$C_{10}H_{14}$ butylobenzene	1351	0.862	29.38	39.6
$C_6H_5NO_2$ nitrobenzene	1475	1.206	43.9	40.5
C_6H_7N aniline	1659	1.022	42.9	39.5
C_7H_9N m-toluidine	1594	0.989	38.3	41.2
C_7H_9N o-toluidine	1618	0.999	40.8	39.6

Table 2, ctd.

1	2	3	4	5
C_7H_9N methylaniline	1586	0.984	39.6	39.4
$C_7H_7NO_2$ o-nitrotoluene	1473	1.163	41.67	41.1
$C_8H_{11}N$ dimethylaniline	1509	0.956	36.6	39.4
$C_5H_{11}N$ piperidine	1400	0.860	30.64	39.3
C_9H_7N chinoline	1600	1.098	45	39.0
$C_6H_{15}N$ triethylamine	1143	0.730	20.9	39.9
$C_{10}H_{18}$ trans-decaline	1403	0.873	29.89	41.0
$C_{10}H_{18}$ cis-decaline	1451	0.895	32.18	40.3
$C_{10}H_{12}$ tetraline	1484	0.969	36.2	39.7
C_7H_{16} 2,2,3-trimethylbutane	1101.5	0.6901	18.86	40.3
C_7H_{16} 3-methylhexane	1135.5	0.687	19.56	39.9
C_7H_{16} 2-methylhexane	1120	0.6789	19.21	39.6
C_7H_{16} 2,4-dimethylpentane	1083.5	0.6745	18.12	40.3
C_7H_{16} 2,3-dimethylpentane	1148.5	0.6942	19.82	40.2
C_7H_{16} 3-ethylpentane	1169.5	0.6982	20.46	39.9

Table 3. N of esters (at 20°C)

Ester	c [m/s]	ϱ [g/cm^3]	σ [dynes/cm]	N
$C_3H_6O_2$ ethyl formate	1160	0.917	23.84	44.6
$C_3H_6O_2$ methyl acetate	1182	0.934	24.49	45.1
$C_4H_8O_2$ propyl formate	1192	0.906	24.5	44.1
$C_4H_8O_2$ ethyl acetate	1177	0.9005	23.9	44.3
$C_5H_{10}O_2$ propyl acetate	1198	0.887	24.3	43.7
$C_5H_{10}O_2$ ethyl propionate	1183	0.890	24.27	43.4
$C_6H_{12}O_2$ ethyl butyrate	1197	0.879	24.58	42.8
$C_8H_8O_2$ methyl benzoate	1472	1.088	37.6	42.6
$C_9H_{10}O_2$ ethyl benzoate	1463	1.047	35.5	43.1

Table 4. N of organic liquids containing bromine in the molecule (m = 79.9) at 20°C

Substance	% by weight of bromine in the molecule	c [m/s]	ϱ [g/cm^3]	σ [dynes/cm]	N
$CHBr_3$ bromoform	94.8	931	2.890	31.68	84.9
$C_2H_2Br_4$ 1,1,2,2-tetrabromethane	92.5	1041	2.967	49.6	62.3
$C_2H_4Br_2$ ethylene bromide	85.1	1009	2.178	38.37	57.3
C_2H_5Br ethyl bromide	73.3	900	1.461	24.15	54.4
C_4H_9Br n-butyl bromide	58.3	1019	1.274	26.33	49.3
C_6H_5Br bromobenzene	50.9	1170	1.495	36.5	47.9
$C_8H_{17}Br$ n-octyl bromide	41.4	1182	1.166	28.89	47.7
$C_{10}H_7Br$ bromonaphthalene	38.6	1372	1.487	44.64	45.7

Table 5. N of organic liquids containing chlorine in the molecule ($m = 35.4$) at 20°C

Substance	% by weight of chlorine in the molecule	c [m/s]	ϱ [g/cm^3]	σ [dynes/cm]	N
CCl_4 carbon tetrachloride	92.2	938	1.594	35.68	58.2
$CHCl_3$ chloroform	89.1	1001	1.487	27.1	54.9
C_2HCl_5 pentachloroethane	87.6	1113	1.672	34.6	53.8
C_2Cl_4 tetrachloroethylene	85.5	1063*)	1.618*)	32.32	53.2
$C_2H_2Cl_4$ tetrachloroethane	84.5	1170	1.595	35.2	53.0
CH_2Cl_2 methylene chloride	83.5	1093	1.318	27.1	53.1
C_2HCl_3 trichloroethylene	81.0	1055*)	1.464*)	29.5	52.4
$C_2H_3Cl_3$ 1,1,1-trichloroethane	79.7	992*)	1.333*)	25.56	51.7
$C_2H_4Cl_2$ 1,2-dichloroethane	71.5	1216	1.252	32.23	47.2
$C_3H_6Cl_2$ 1,2-dichloropropane	62.8	1162	1.155	28.65	46.8
C_3H_7Cl 1-chloropropane	45.1	1091	0.890	22.0	44.1
C_4H_9Cl chlorobutane	38.3	1140	0.885	23.66	42.6
C_6H_5Cl chlorobenzene	31.5	1289	1.104	33.2	42.9

*) according to measurements made by the author

Table 6. N as function of temperature for mercury

°C	c [m/s]	ϱ [g/cm³]	σ [dynes/cm]	N
0	1460.2	13.5955	479.5	41.40
10	1455.6	13.5708	477	41.41
20	1451.0	13.5462	475	41.38
25	1448.7	13.5340	473.5	41.41
30	1446.4	13.5212	472.5	41.39
40	1441.7	13.4967	470	41.40
50	1437.1	13.4729	467.5	41.42
100	1413.9	13.3522	456	41.40
150	1390.7	13.232	444	41.44
200	1367.5	13.1148	433	41.42
250	1344.3	12.994	416	41.99
300	1321.1	12.8806	400	42.54
350	1297.9	12.757	381	43.46

If both sides of this equation are divided by $\Delta t = t_2 - t_1$, we obtain a formula from which $\Delta c/\Delta t$ can be evaluated without any information about the o und velocity of a given liquid:

$$\frac{\Delta c}{\Delta t} = \frac{N}{t_2 - t_1}\left(\frac{\sigma_1}{\varrho_1} - \frac{\sigma_2}{\varrho_2}\right). \tag{2}$$

It is a common practice to quote the sound velocity in a given liquid at a certain temperature (most tables state values at 20°C). Thus only the coefficient $\Delta c/\Delta t$ is unknown, and different sources state different values. Substituting the value of $N = c_1 \varrho_1/\sigma_1$ into formula (2), we get

$$\frac{\Delta c}{\Delta t} = \frac{c_1}{t_2 - t_1}\left(1 - \frac{\varrho_1 \sigma_2}{\varrho_2 \sigma_1}\right). \tag{3}$$

Calculations have been made using formulae (2) and (3) for 10 typical organic liquids. The results of these calculations, and also the measured values of $\Delta c/\Delta t$ compiled by SCHAAFFS are given in Table 7.

On the basis of the analysis of the data contained in Table 7 and other data, not cited in this paper, it can be concluded that using the quoted formulae

it is possible to calculate, with good accuracy, the temperature coefficient of sound velocity in organic liquids, provided that:

– the numerical values from which the coefficient $\Delta c/\Delta t$ is evaluated must be extremely accurate (the accuracy of the surface tension in particular should be at least 0.01 dynes/cm),

– the temperature range Δt is as wide as possible.

Table 7. Comparison of calculated and measured values of $\Delta c/\Delta t$ for 10 organic liquids

Liquid	Data used for calculations				$\Delta c/\Delta t$ [m/s·deg] calculated[1)]	$\Delta c/\Delta t$ [m/s·deg] measured
	t[°C]	ϱ[g/cm³]	σ[dynes/cm]	c[m/s]		
1	2	3	4	5	6	7
Hexane C_6H_{14}	20	0.6594	18.41	1083	4.74	4.4^{50}_{10}
	60	0.6221	14.33	—	4.72	
Heptane C_7H_{16}	20	0.68276	20.29	1154	4.33	4.0^{90}_{0}
	90	0.6236	13.64	—	4.29	4.14^{50}_{0}
Octane C_8H_{18}	20	0.7022	21.78	1192	4.04	3.95^{100}_{20}
	120	0.6168	12.64			4.22^{50}_{0}
Benzene C_6H_6	20	0.8790	28.87	1324	4.55	4.48^{80}_{10}
	80	0.8145	21.24	—	4.51	4.60^{70}_{10}
						4.78^{50}_{10}
Toluene $C_6H_5CH_3$	20	0.8669	28.53	1328	4.24	4.30^{50}_{0}
						4.30_{10}
o-xylene $C_6H_4(CH_3)_2$	20	0.8801	30.03	1364	3.81	3.80^{100}_{20}
	100	0.8029	21.27	—	3.81	
Methanol CH_3OC	20	0.7915	22.55	1123	3.08	3.23^{60}_{20}
	50	0.7650	20.0	—	3.18	3.25^{50}_{0}
						3.26^{50}_{0}
						3.3^{30}_{10}
Ethanol C_2H_5OH	20	0.7894	22.55	1159	3.37	3.15^{70}_{20}
	50	0.76315	19.9	—	3.38	3.16^{70}_{20}
						3.4^{30}_{10}
						3.50^{50}_{0}
Methyl acetate $CH_3COO.CH_3$	20	0.9338	24.49	1182	4.92	4.6^{30}_{10}
	30	0.92065	23.14	—	4.77	4.73^{50}_{10}
Ethyl acetate $CH_3COO.C_2H_5$	20	0.9005	23.9	1177	4.65	4.5^{30}_{10}
	50	0.8635	20.2	—	4.58	4.88^{50}_{10}

[1)] the upper value has been calculated from formula (3), the lower value – from formula (2).

Table 8. Comparison of calculated and measured values of surface tension at various temperatures for fifteen organic liquids

Liquid	$\frac{\Delta c}{\Delta t}$ [m/s·deg] used for calculations	t [°C]	σ measured [dynes/cm]	σ calculated [dynes/cm]
1	2	3	4	5
Hexane C_6H_{14}	4.4_{10}^{50}	60	14.33	14.55
Heptane C_7H_{16}	4.14_{0}^{50}	90	13.64	13.86
Octane C_8H_{18}	3.95_{20}^{100}	120	12.64	12.79
Benzene C_6H_6	4.60_{10}^{70}	80	21.24	21.17
Toluene $C_6H_5 \cdot CH_3$	4.30_{0}^{50}	40	26.13	26.10
o-Xylene $C_6H_4 \cdot (CH_3)_2$	3.80_{20}^{100}	100	21.27	21.29
Methanol CH_3OH	3.25_{0}^{50}	50	20.0	19.90
Ethanol C_2H_5OH	3.50_{10}^{50}	50	19.9	19.82
Methyl acetate $CH_3COO \cdot CH_3$	4.73_{10}^{50}	30	23.14	23.18
Ethyl acetate $CH_3COO \cdot C_2H_5$	4.88_{10}^{50}	50	20.2	20.07
Carbon tetrachloride CCl_4	3.30_{0}^{50}	100	16.48	16.60
Chlorobenzene C_6H_5Cl	3.70_{0}^{50}	50	29.6	29.38
Dichloropropane $C_3H_6Cl_2$	3.80_{0}^{60}	60	23.8	23.80
Trichloroethylene C_2HCl_3	3.5_{20}^{30}	60	24.4	24.36
Tetrachloroethylene C_2Cl_4	3.3_{15}^{30}	60	26.9	26.99

Note. In the two last items $\Delta c/\Delta t$ according to the author's measurements

Attention should be drawn to the rather frequently occurring discrepancies in the numerical data for the surface tension from different sources. It would appear that formulae presented here can be used for the verification of these data. Furthermore, it is possible to calculate the surface tension of organic liquids for cases where the value of σ for a given temperature is unknown. For this purpose suitable transformations of formulae (1) and (3) are used:

$$\sigma = \frac{\varrho c}{N}, \tag{4}$$

$$\sigma_2 = \frac{\sigma_1 \varrho_2}{\varrho_1}\left(1 - \frac{\Delta c}{\Delta t}\frac{t_2 - t_1}{c_1}\right). \tag{5}$$

The values obtained with the aid of these formulae do not in most cases differ by more than 0.3 dynes/cm from measured values of the surface tension. For practical purposes this accuracy is quite satisfactory. In Table 8 the results of calculations according to formula (5) are compared with values of the surface tension obtained by the direct measurement.

References

[1] J. A. TREGHIER, I. F. PIMIENOV, J. A. GOLFAND, *Handbook on physico-chemical properties of aliphatic chlorine bonds C_1-C_5* [in Russian], Khimiia, Leningrad 1973.

[2] *Physico-chemical handbook* [in Polish], WNT, Warszawa 1974.

[3] *Chemist's handbook* [in Russian], vol. I and II, Goschimizdat, Leningrad-Moscow 1962 and 1963.

[4] W. SCHAAFFS, *Atomic and molecular physics*, Volume 5: Molecular Acoustics, Landolt-Bornstein new series. Group II. Springer Verlag, Berlin-Heidelberg-New York 1967.

Received 4th February 1976

C H R O N I C L E

2ND SYMPOSIUM ON THE APPLICATION OF VIBRATION AND NOISE IN THE DIAGNOSTIC INVESTIGATION OF MACHINES

Porąbka near Żywiec, March 22-27, 1976

The promotor of the Symposium was the Institute of Transport and Communications of Silesian Technical University in Katowice. Professor Ludwik MÜLLER was responsible for the scientific programme. 13 lectures were delivered and discussed by the following scientific centres: the Academy of Mining and Metallurgy, the Agricultural Academy in Lublin, the Technical Institute of the Air Force, the Institute of Motor Transport, the R & D Centre of the Katowice Metallurgical Plant, the R & D section of Zygmunt Metallurgical Plant, R & D section of a Small Capacity Car Factory, Silesian Technical University, Świętokrzyski Technical University, Poznań Technical University, Warsaw Technical University, the Naval College, the Engineering College in Zielona Gora, the Military College of Armour and Automotive Engineering, the Higher Officer Automotive College, and Agromet in Poznań.

The symposium was greatly appreciated by the participants. During the main debate it was suggested that the Institute of Transport and Communications of the Silesian Technical University should organize scientific meetings devoted to the problems discussed.

Józef Przybylski (*Katowice*)

SIGNING OF AN AGREEMENT ON SCIENTIFIC COOPERATION BETWEEN THE POLISH ACOUSTICAL SOCIETY (PTA) AND THE GROUPEMENT DES ACOUSTICIENS DE LANGUE FRANÇAISE (GALF)

On March 3rd, 1976, an agreement on scientific cooperation was signed between the Polish Acoustical Society (PTA) and the Groupement des Acousticiens de Langue Française (GALF). The ceremony took place in Warsaw in the Palace of Culture and Science. The authorities of the Polish Academy of Sciences were represented by Prof. Maciej NAŁĘCZ, Secretary of Division IV of the Polish Academy of Sciences (PAN).

Also the members of the Presidium of the Main Board of the PTA and the Presidium of the Acoustics Committee on Acoustics of PAN and representatives of the Foreign Cooperation Bureau of the PAN and of the French Embassy in Warsaw were present.

After a short welcome and address by Prof. NAŁĘCZ, the official signing of the agreement took place. The agreement was signed on behalf of the Polish Acoustical Society by Halina RYFFERT, President of the Society, and on behalf of the Groupement des Acousticiens de Langue Française, by Paul FRANÇOIS, President of GALF. The signatories to the agreement

then delivered speeches. Both speeches included elements evidencing the development of existing contacts, as well as the possibility of concrete cooperation between the societies. To a great extent the promotor of the formalization of this cooperation was Leonid PIMONOV, the former President of GALF who, three years ago, suggested the need for an advisability of signing a formal agreement between our societies. Mr. Paul FRANÇOIS was the continuator of this idea and as a result of this consistent cooperation with the President of PTA the final text of the agreement was been formulated to the satisfaction of both societies and, finally, led to the signing of the agreement.

The letter from the Main Board of PTA was handed to the wife of Leonid PIMONOV, Mrs. Eugene PIMONOV, with thanks for the initiative and assistance in establishing the cooperation.

GREAT MEDAL OF GALF FOR PROFESSOR HALINA RYFFERT

On February 28th, 1976, the President of GALF – Paul FRANÇOIS, presented a great medal of GALF to Halina RYFFERT, the President of the Polish Acoustical Society. Such medals are awarded every year to two persons, one living outside French territory, for special merits in the encouragement of scientific cooperation with France in the field of acoustics.

The ceremony took place during the conclusion of the scientific session on the occasion of the 20th anniversary of Chair of Acoustics at A. Mickiewicz University in Poznań.

President of GALF – Paul François is presenting a great medal of GALF to Halina Ryffert